

Accepted Manuscript

Rational design, synthesis and biological screening of triazine-triazolopyrimidine hybrids as multitarget anti-Alzheimer agents

Ehtesham Jameel, Poonam Meena, Mudasir Maqbool, Jitendra Kumar, Waqar Ahmed, Syed Mumtazuddin, Manisha Tiwari, Ph.D., Assistant Professor, Nasimul Hoda, Ph.D., Professor, B. Jayaram

PII: S0223-5234(17)30338-0

DOI: [10.1016/j.ejmech.2017.04.064](https://doi.org/10.1016/j.ejmech.2017.04.064)

Reference: EJMECH 9415

To appear in: *European Journal of Medicinal Chemistry*

Received Date: 26 January 2017

Revised Date: 2 April 2017

Accepted Date: 23 April 2017

Please cite this article as: E. Jameel, P. Meena, M. Maqbool, J. Kumar, W. Ahmed, S. Mumtazuddin, M. Tiwari, N. Hoda, B. Jayaram, Rational design, synthesis and biological screening of triazine-triazolopyrimidine hybrids as multitarget anti-Alzheimer agents, *European Journal of Medicinal Chemistry* (2017), doi: 10.1016/j.ejmech.2017.04.064.

This is a PDF file of an unedited manuscript that has been accepted for publication. As a service to our customers we are providing this early version of the manuscript. The manuscript will undergo copyediting, typesetting, and review of the resulting proof before it is published in its final form. Please note that during the production process errors may be discovered which could affect the content, and all legal disclaimers that apply to the journal pertain.



**Rational design, synthesis and biological screening of
triazine-triazolopyrimidine hybrids as multitarget anti-Alzheimer agents**

Ehtesham Jameel^a, Poonam Meena^b, Mudasir Maqbool^a, Jitendra Kumar^a, Waqar Ahmed^a, Syed Mumtazuddin^c, Manisha Tiwari^{b*}, Nasimul Hoda^{a*} and B. Jayaram^{d,e,f}

^aDepartment of Chemistry, Jamia Millia Islamia (Central University), Jamia Nagar, New Delhi 110025, India

^bDr. B. R. Ambedkar Centre for Biomedical Research, University of Delhi, New Delhi 110007, India

^cDepartment of Chemistry, B. R. Ambedkar Bihar University, Muzaffarpur 842001, Bihar, India

^dDepartment of Chemistry, Indian Institute of Technology Delhi, Hauz Khas, New Delhi 110016, India

^eKusuma School of Biological Sciences, IIT Delhi, New Delhi 110016, India

^fSupercomputing Facility for Bioinformatics & Computational Biology, IIT Delhi, New Delhi 110016, India.

* Corresponding authors.

#Nasimul Hoda, Ph.D.

Professor
Department of Chemistry
Jamia Millia Islamia,
Jamia Nagar, New Delhi-110025,
India
Email: nhoda@jmi.ac.in

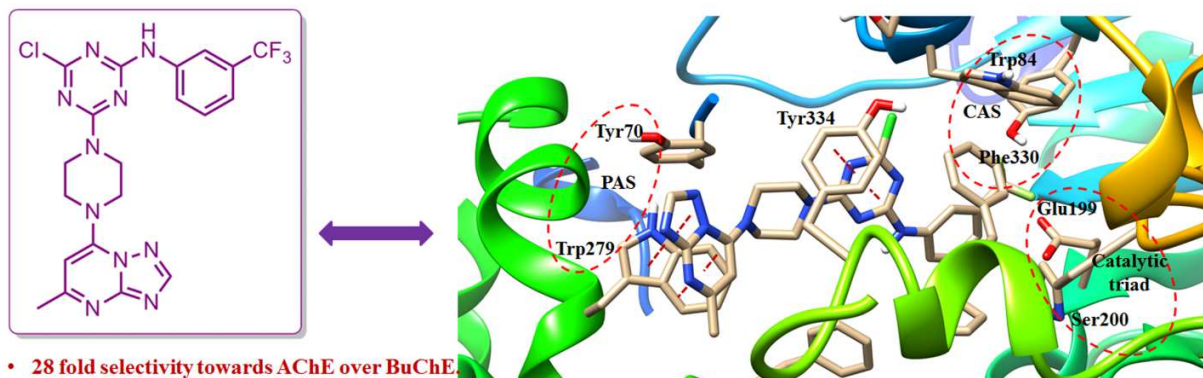
\$Manisha Tiwari, Ph.D.

Assistant Professor
Dr. B. R. Ambedkar
Centre for Biomedical Research,
University of Delhi, New Delhi-110007,
India
Email: mtiwari07@gmail.com

Research highlights:

- A series of triazine-triazolopyrimidine hybrids were designed and synthesised.
- Docking studies revealed that compounds 9a and 9b had appreciable binding free energies and affinities with AChE.
- The most promising compound (**9a**) had an inhibition selectivity of ~28 fold against AChE over BuChE.
- A β_{1-42} disaggregation, metal binding studies, CD spectroscopic, ADME property and TOPKAT analysis were also performed.

Graphical Abstract



ACCEPTED MANUSCRIPT

Abstract

In our endeavor towards the development of potent multitarget ligands for the treatment of Alzheimer's disease, a series of triazine-triazolopyrimidine hybrids were designed, synthesized and characterized by various spectral techniques. Docking and scoring techniques were used to design the inhibitors and to display their interaction with key residues of active site. Organic synthesis relied upon convergent synthetic routes where mono and di-substituted triazines were connected with triazolopyrimidine using piperazine as a linker. In total, seventeen compounds were synthesized in which the di-substituted triazine-triazolopyrimidine derivatives **9a-d** showed better acetylcholinesterase (AChE) inhibitory activity than the corresponding tri-substituted triazine-triazolopyrimidine derivatives **10a-f**. Out of the disubstituted triazine-triazolopyrimidine based compounds, **9a** and **9b** showed encouraging inhibitory activity on AChE with IC_{50} values 0.065 and 0.092 μ M, respectively. Interestingly, **9a** and **9b** also demonstrated good inhibition selectivity towards AChE over BuChE by ~28 folds. Furthermore, kinetic analysis and molecular modeling studies showed that **9a** and **9b** target both catalytic active site as well as peripheral anionic site of AChE. In addition, these derivatives effectively modulated $A\beta$ self-aggregation as investigated through CD spectroscopy, ThT fluorescence assay and electron microscopy. Besides, these compounds exhibited potential antioxidants (2.15 and 2.91 trolox equivalent by ORAC assay) and metal chelating properties. *In silico* ADMET profiling highlighted that, these novel triazine derivatives have appropriate drug like properties and possess very low toxic effects in the primarily pharmacokinetic study. Overall, the multitarget profile exerted by these novel triazine molecules qualified them as potential anti-Alzheimer drug candidates in AD therapy.

Keywords: Alzheimer's disease, Acetylcholinesterase, Butyrylcholinesterase, Triazine, Triazolopyrimidine quinoline, Molecular docking, ADME analysis.

ACCEPTED MANUSCRIPT

1. Introduction

Alzheimer's disease (AD) is an age related irreversible neurodegenerative disorder characterized by memory loss [1]. About 46.8 million people have been reported to suffer globally in 2015 from AD which is expected to increase by three fold in 2050 [2]. No such treatment has yet been developed that could prevent, cure or even slow down the progress of this disorder. It is the third leading cause of death after cardiovascular disease and cancer globally. The mechanism of this dementia has not been fully elucidated due to multifactorial progression and complex etiology. Since, its exact etiology is unclear, current evidence suggests that the abnormal accumulation of amyloid- β ($A\beta$) and tau protein in the form of neurofibrillary tangles (NFTs) are the main hallmark of AD [3]. $A\beta$ is produced by the proteolytic break down of amyloid precursor protein (APP), a transmembrane protein by the action of β - and γ -secretases [4]. NFTs are formed by the hyperphosphorylation of microtubule associated protein called tau which is overseen by overexpression of GSK-3 β [5]. Beside this, decrease of acetylcholine (ACh) an important neurotransmitter is also associated with the symptoms of dementia and learning difficulties. A serine hydrolase enzyme called acetylcholinesterase (AChE), promotes the breakdown of ACh. Drugs that target the clearing or preventing the formation of $A\beta$ and NFTs can prove to be a successful approach towards the treatment of AD. Donepezil, rivastigmine, galantamine, and tacrine are some FDA approved acetylcholinesterase inhibitors (AChEIs) used for the treatment of AD. These AChEIs lack the long-term efficacy and possess side effects, like, gastrointestinal disturbance, hepatotoxicity, dizziness, liver damage, vomiting and nausea [6]. The limited clinical efficacy of these approved drugs further propel medicinal chemists to put their efforts towards the development of molecules that can simultaneously hit multiple targets of AD etiology.

1,3,5-Triazine scaffold has a great history for the fabrication of antiviral [7], antifungal [8], antimalarial [9], antibacterial [10], and anticancer agents [11][12]. Recently, a group of 2,4,6-trisubstituted 1,3,5-triazine compounds was found to be effective against various cysteine cathepsins with endopeptidase activity [13]. One more important pharmacological usage of substituted 1,3,5-triazines has been explored that these compounds possess the antagonist selectivity effect against adenosine receptors [14]. There are many more effects of triazine analogues [15], so to say triazine is a fertile moiety and has been serving medicinal chemists for a long time. The triazine and its derivatives could be synthesized via feasible convergent synthetic route. Since, triazine possesses a roughly planar structure and was expected to favor the A β disaggregation. Triazolopyrimidine scaffold was expected to engage with the important residues at PAS of AChE, so could enhance the ability of the drug molecules to inhibit the enzyme. Indeed, triazole scaffold has been efficiently utilized in the design of multifunctional AChEIs [16]. Since the active site of AChE is roughly 20 Å deep narrow gorge encrusted primarily by aromatic residues, so piperazine as a linker between the two main moieties was expected to increase the length of the drug molecule and engage with in π -cation interaction with the aromatic gorge. Hence, combined scaffolds of quinoline and triazolopyrimidine through piperazine was preferred choice due to their various valuable properties. In our previous work we attempted to evaluate these two moieties separately for the development of anti-AD drugs [17] [18].

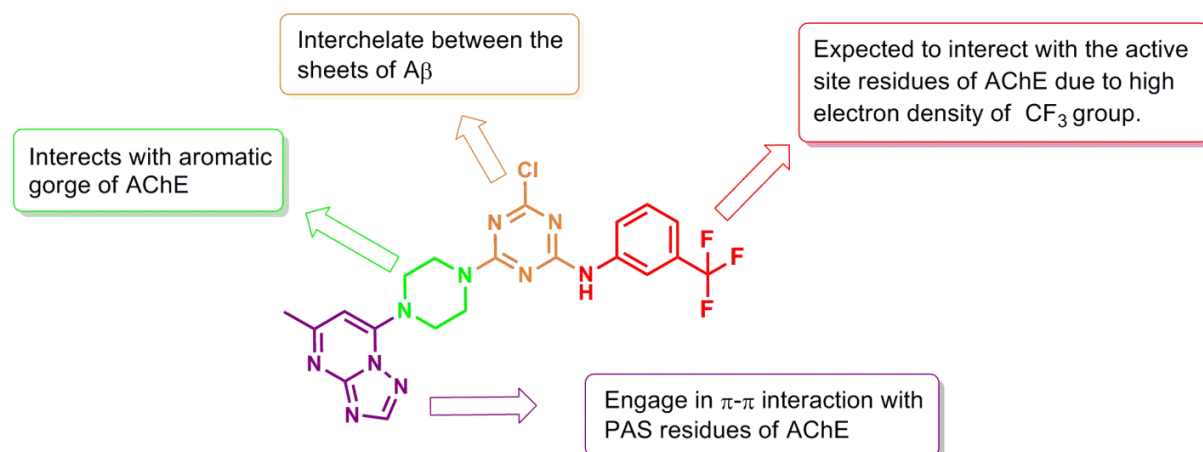


Fig. 1. Design of multifactorial anti-AD agent

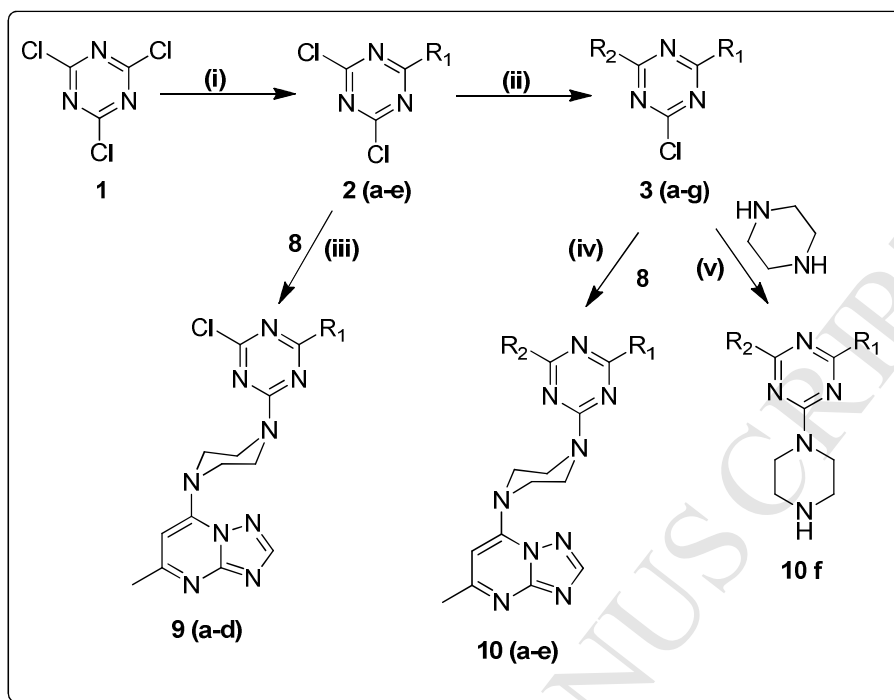
Herein, a series of seventeen compounds was designed and synthesized. *In vitro* inhibitory activity towards cholinesterases and A β disaggregating ability of all the synthesized compounds were assessed. Further, the mechanism of AChE inhibition was investigated by kinetic studies. In order to obtain a better understanding of possible interactions with biological targets, molecular docking studies and binding free energy calculations were also performed.

2. Results and Discussion

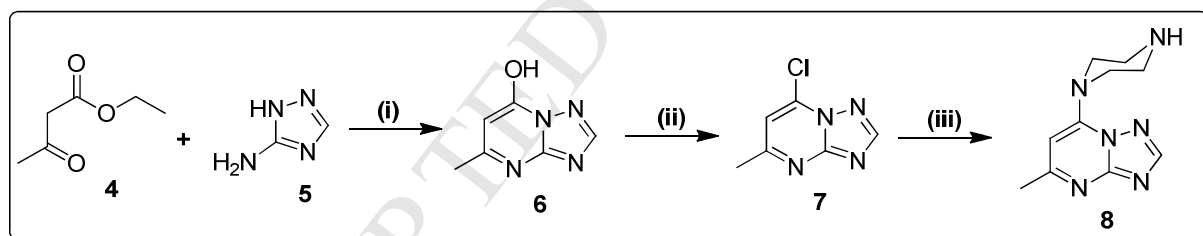
2.1. Chemistry

The synthesis of the target molecules were achieved by multistep reactions which are outlined in **Scheme 1 and 2**. The triazine derivatives of the intermediate compounds i.e. mono and disubstituted compounds **2a-e** and **3a-g** were synthesized by the reported literature[17]. The cyanuric chloride was first reacted with 3-(trifluoromethyl)aniline, p-anisidine, p-fluoroaniline, o-fluoroaniline and 3-chloro-4-fluoroaniline at -10 °C in THF and K₂CO₃ to obtain monosubstituted compounds. The obtained monosubstituted compounds were treated with different amines to get **3a-g** as disubstituted compounds. Synthetic route for the synthesis of **8**, i.e. 1-{5-methyl- [1,2,4]triazolo[1,5-a]pyrimidin-7-yl} piperazine attached to triazine derivatives

of the mono and disubstituted compounds have been depicted in Scheme 2. Finally, the monosubstituted triazine derivatives **2a-e** were treated with **8** in the presence of K_2CO_3 and 1,4-dioxane at room temperature in N_2 medium to obtain the target compounds di-substituted triazine triazolopyrimidine piperazine as **9a-d**. Similarly, the disubstituted triazine compounds **3a-g** were also treated with **8** in presence of K_2CO_3 and 1,4-dioxane at $110\text{ }^\circ\text{C}$ in N_2 medium to obtain the tri-substituted triazine triazolopyrimidine piperazine **10a-e** as desired compounds. In these schemes we see that the reactions involved in the synthesis of the target compounds were temperature dependent nucleophilic aromatic substitution reactions. The intermediates i.e. monosubstituted triazines were synthesized at -5 to $-10\text{ }^\circ\text{C}$, disubstituted at room temperature while the final or the targeted compounds were obtained at higher temperature, i.e., $110\text{ }^\circ\text{C}$. Finally, all the newly synthesized compounds were stable enough to be isolated by column chromatography on silica gel and their structures were unambiguously verified by different elemental analysis and spectroscopic data i.e. ^1H NMR, ^{13}C NMR, ESI MS and CHNS.



Scheme: 1. *Reagents and conditions:* (i) aromatic amines, tetrahydrofuran (THF), -10 °C, K_2CO_3 (ii) aliphatic/ aromatic amines, THF, room temperature, K_2CO_3 , (iii) K_2CO_3 , 1,4-dioxane, room temperature, N_2 ; (iv) & (v) 1,4-dioxane, K_2CO_3 , 100 °C, N_2 .



Scheme: 2. *Reagents and conditions:* (i) Acetic acid, 110 °C; (ii) $POCl_3$, 110 °C; (iii) piperazine, K_2CO_3 , 1,4-dioxane, 100 °C.

Compound	R ₁
2 (a)	
2 (b)	
2 (c)	
2 (d)	
2 (e)	
9 (a)	
9 (b)	
9 (c)	
9 (d)	

Compound	R ₁	R ₂
3 (a)		
3 (b)		
3 (c)		
3 (d)		
3 (e)		
3 (f)		
3 (g)		
10 (a)		
10 (b)		
10 (c)		
10 (d)		
10 (e)		
10 (f)		

2.2. Molecular modeling studies

Structure based drug design approach was used to obtain an influential drug candidate for multi-faceted AD. Triazine, because of its roughly planar structure was selected as a preferred scaffold. It was expected to interpolate between beta-amyloid sheets was expected to minimize the beta-amyloid aggregation. Due to the aromaticity of triazine, it was also expected to engage efficiently with the active site residues of AChE via π - π stacking interaction and alkyl- π -interaction. Substitution of triazine with p-anisidine was a natural choice because anisidine is known to have neuroprotective and radical scavenging effect [19]. Piperazine was incorporated in order to connect two electrophilic centres and its nitrogen was expected to be in protonated state and hence may participate in π -cation interactions with the residues of aromatic gorge. ParDock module of *Sanjeevini* (SCFBIO, IITD) [20][21] was selected for docking and scoring purposes. The computational binding free energy of synthesized molecules and reference compound donepezil with AChE and BuChE is provided in **Table 1**. The Binding free energy (ΔG in kcal/mol) of compounds **9a**, **9b** and **donepezil** for AChE was found to be **-10.87**, **-10.53** and **-7.85** respectively, which proposes a very high binding affinity for 9a and 9b between the ligands and the enzyme but least with the donepezil. Binding free energy value i.e. -10.32, -9.93 and -6.07 kcal/mol of compounds **9a**, **9b** and **donepezil** for BuChE was also recorded. All the synthesized molecules revealed more inhibition selectivity for AChE over BuChE.

A docking study was executed on reported crystal structure of AChE with PDB ID 1EVE. Better interaction of compounds **9a** and **9b** for AChE was predicted and same results were obtained via their docking studies. In **Fig. 2(a)** and **2(b)** aromatic ring of Tyr334 was expected to show π - π stacking with the triazine core moiety of both compound **9a** and **9b**, respectively. Triazolopyrimidine bicyclic system of compound **9a** was found to have the aryl- π interaction

with the bicyclic system of Trp279 which is located at the peripheral anionic site of AChE. In **Fig. 2(b)** Trp84 interact with Triazolopyrimidine of compound **9b** via π - π stacking.

The results of docking study publicized that the dual binding activity for selected compound may be due to π - π (aromatic) interactions with CAS and PAS of AChE.

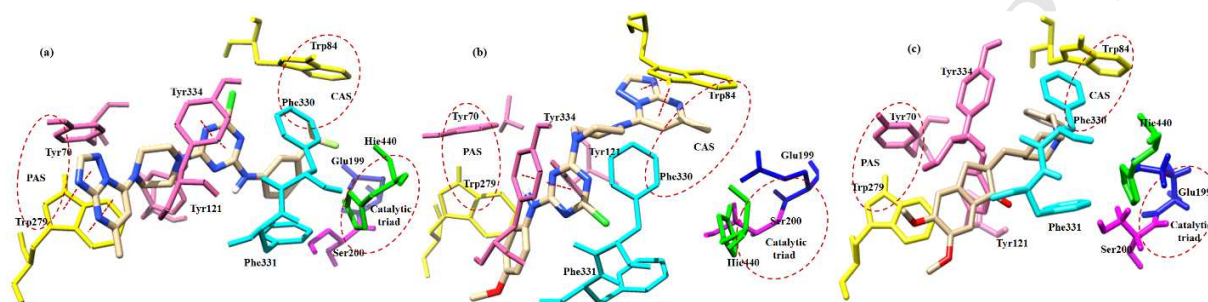


Fig. 2. (a), (b) and (c) are the docked inhibitors of compound **9a**, **9b** and donepezil with AChE. Interactions with key residues are shown in different colors. Tyr with hot pink, Trp in yellow, Phe in cyan, His in green, Glu in blue and Ser in magenta color. π - π stacking are shown in red dashed lines.

Docking studies were further extended to the reported crystal structure of Human BuChE (PDB ID 4TPK) with the synthesized compounds. The docked structures of best resulting compounds (**9a** and **9b**) and **donepezil** as a reference compound are given in **Fig. 3(a)**, **3(b)** and **3(c)** respectively. 3-trifluoromethyl aniline of compound **9a** and p-anisidine of compound **9b** was found to have the aryl- π interaction with the bicyclic system of Trp82 which is located at the catalytic anionic site of AChE. Aromatic ring of Tyr332 was expected to interact with the piperazine ring of compound **9a** and π - π stacking of triazolopyrimidine bicyclic system with compound **9b**, respectively. However, the calculated free binding energies of the synthesized molecules suggested their more selectivity for AChE over BuChE as shown in **Table 1**.

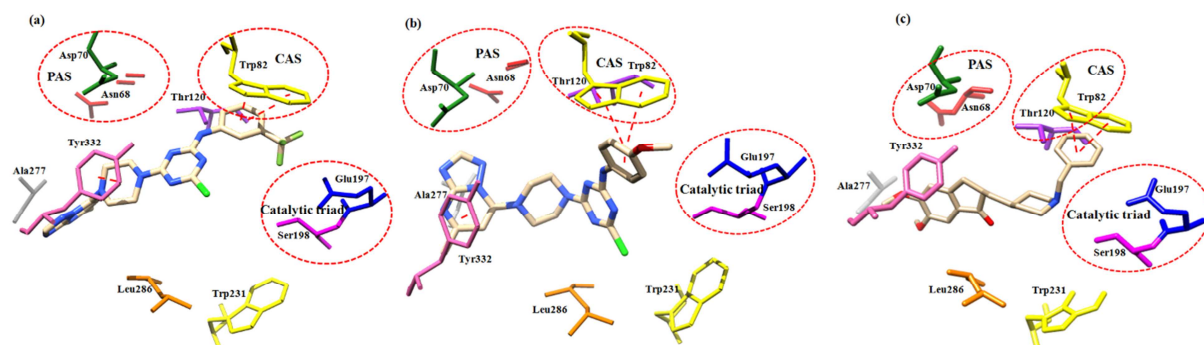


Fig. 3. (a), (b) and (c) are the docked inhibitors of compound **9a**, **9b** and **donepezil** with BuChE. Interactions with key residues are shown in different colors. Tyr with hot pink, Trp in yellow, Glu in blue and Ser in magenta, Thr in purple, Asp in forest green, Asn in red, Ala in dark grey, and Leu in orange color. π - π stacking are shown in red dashed lines.

Table 1. Calculated free energy values of the docked compounds by ParDock[20]

Compounds	Free energy values	Free energy values
	(kcal/mol) AChE	(kcal/mol) BuChE
9a	-10.87	-10.32
9b	-10.53	-9.93
9c	-9.12	-8.85
9d	-8.15	-7.31
10a	-9.16	-8.14
10b	-9.75	-8.34
10c	-9.84	-8.67
10d	-9.35	-7.98
10e	-8.98	-7.73
10f	-9.02	-7.81
3a	-8.71	-7.41
3b	-8.53	-7.18
3c	-8.19	-6.91
3d	-8.34	-7.39
3e	-8.83	-7.58
3f	-7.68	-6.32
3g	-7.82	-6.75
Donepezil	-7.85	-6.07

Bolded values depict the most active compounds **9a** and **9b**.

2.3. Pharmacological evaluation

2.3.1. *In vitro* AChE and BuChE inhibitory activity

The inhibitory activity of triazine derivatives **9a-d**, **3a-g** and **10a-f** was evaluated *in vitro* against AChE (from *Electrophorus electricus*) and BuChE (from equine serum) using Ellman's method [22]. Donepezil and tacrine were used as reference standards for comparative analysis. The corresponding IC₅₀ values of all the synthesized derivatives are listed in **Table 2**. Most of the target compounds displayed significant inhibitory activities against both cholinesterases (ChEs) with IC₅₀ values in micromolar range. Structure activity relationship (SAR) studies indicated that the ChE inhibition and selectivity were sensitive to substituents with different electronic properties on the core triazine scaffold. Within the series, it was observed that the di-substituted triazine derivatives **9a-d** displayed better AChE inhibition than the corresponding tri-substituted derivatives **10a-f**. Interestingly, compound **9a** with trifluoromethyl substitution at the C-3 position of phenyl ring exhibited the most potent AChE inhibitory activity with IC₅₀ value of 0.065 μM, which was ~3.5-fold stronger than the reference compound tacrine. In addition, **9a** also demonstrated a high selectivity for AChE over BuChE (~28-fold). The presence of methoxy substituent at C-4 position of phenylamine moiety in **9b** also revealed notable selective inhibition towards AChE (IC₅₀ = 0.092 μM and S.I = ~ 16). In case of **9c**, the introduction of fluoro group at C-4 position also showed significant inhibition against AChE with IC₅₀ values of 0.115 μM, while the BuChE inhibitory activity improved slightly (IC₅₀ = 0.93 μM). The presence of fluoro group at C-2 position of phenylamine moiety attached to C-2 of heteroaromatic triazine (**9d**) core led to reduce AChE activity as compared to the lead compound **9a**. In the tri-substituted-1,3,5-triazine derivatives, a range of substituents were varied over the phenyl amine ring. In case of

compounds **10a** and **10b**, trifluoromethyl substitutions at the C-3 position were kept constant and variations were performed at other terminal end. The presence of cyclopropane ring in **10a** ($IC_{50} = 0.903 \mu M$) was observed to be unfavorable for ChE inhibition in comparison to the methylbenzene moiety (**10b**, $IC_{50} = 0.558 \mu M$). The combined introduction of Cl and F at C-3 and C-4 position of the phenyl ring (**10c**) gave more potent AChE inhibition ($IC_{50} = 0.338 \mu M$) with respect to fluoro substituent at C-4 (**10d**, $IC_{50} = 0.724 \mu M$). However, absence of triazolo pyrimidine heterocycle at N-4 terminal of piperazine ring (**10f**) lead to a significant loss of inhibitory potency ($IC_{50} = 1.25 \mu M$) which was nearly ~19-fold lower than most potent compound. These results point out towards the relevant role played by the triazolo pyrimidine scaffold on the AChE inhibition which is in consistent with our earlier investigation [18]. The series of di-substituted-1,3,5-triazine derivatives represented by nonsubstituted counterparts **3a-g** at C-4 of the triazine core exerted slightly lower AChE inhibition. In general, it seems that the presence of trifluoromethyl substitution at C-5 of phenylamine ring is particularly favorable for anti-AChE activity. The common trend of substitution observed at the other terminal end of phenylamine moiety was of the order: **3e** [3-Chloro-4-fluorol] > **3a** [2,4-difluoro] > **3b** [4-fluoro] > **3d** [4-methoxy] > **3c** [4-methyl], respectively. In this series, compound **3e** was found to demonstrate a higher inhibitory potency towards AChE with an IC_{50} value of $0.432 \mu M$ which was about ~1.5-fold potent than those of compound **3c**. However, the replacement of substituted trifluoromethyl group with 3-chloro-4-fluoro substituents in compounds **3f** and **3g** has led to significant decrease in AChE inhibitory potencies. In general, most of the target compounds were significantly active for both ChEs with greater selectivity towards AChE over BuChE. Overall the SAR results clearly suggested the influence of electronic and steric properties of substituents on the modulation of ChE inhibition.

Table 2. *In vitro* inhibition of AChE and BuChE, selectivity index and oxygen radical absorbance capacity (ORAC, Trolox equivalents) of the target compounds.

Compounds	AChE ^a IC ₅₀ (μM)	BuChE ^b IC ₅₀ (μM)	Selectivity index ^c BuChE/AChE	Trolox equiv ^d
9a	0.065 ± 0.002	1.88 ± 1.27	28.92	2.15 ± 0.64
9b	0.092 ± 0.001	1.52 ± 0.08	16.52	2.91 ± 0.58
9c	0.115 ± 0.11	0.93 ± 1.03	8.08	1.68 ± 0.52
9d	0.286 ± 0.52	2.23 ± 0.24	7.79	1.14 ± 0.62
10a	0.903 ± 0.30	1.90 ± 0.29	2.10	0.98 ± 0.32
10b	0.558 ± 0.69	1.75 ± 0.75	3.13	1.04 ± 0.38
10c	0.388 ± 0.19	2.614 ± 0.13	6.73	1.37 ± 0.52
10d	0.724 ± 0.26	2.49 ± 0.30	3.43	0.89 ± 0.16
10e	0.859 ± 0.07	3.782 ± 0.22	4.40	0.97 ± 0.35
10f	1.25 ± 0.33	3.65 ± 0.93	2.92	0.80 ± 0.33
3a	0.496 ± 0.09	4.33 ± 0.67	8.72	1.16 ± 0.69
3b	0.526 ± 0.27	2.45 ± 0.91	4.65	1.53 ± 0.82
3c	0.672 ± 0.35	2.09 ± 0.09	3.11	1.20 ± 0.86
3d	0.591 ± 0.092	2.961 ± 0.15	5.01	1.83 ± 0.40
3e	0.432 ± 0.44	3.983 ± 0.52	9.21	1.22 ± 0.39
3f	0.917 ± 0.19	2.77 ± 0.83	3.02	1.62 ± 0.51
3g	0.705 ± 0.08	1.639 ± 0.38	2.32	1.78 ± 0.83
Donepezil	0.047 ± 0.15	2.72 ± 0.09	57.87	n.d ^e
Tacrine	0.226 ± 0.07	0.056 ± 0.14	0.25	n.d ^e

^aAChE from electric eel; IC₅₀, inhibitor concentration (mean ± SD of three independent experiments) resulting in 50% inhibition of AChE.

^bBuChE from equine serum; IC₅₀, inhibitor concentration (mean ± SD of three independent experiments) resulting in 50% inhibition of BuChE.

^cSI selectivity index for AChE: IC₅₀ (EqBuChE)/IC₅₀ (EeAChE).

^dData are expressed as μmol of trolox equivalent/μmol of tested compound.

^en.d, not determined.

2.3.2. Kinetic study of AChE inhibition

To gain further insight into the mode of inhibition of this family of compounds on AChE, kinetic measurements were carried out with the most active inhibitors (**9a** and **9b**) of the series, using EeAChE. The analysis was carried out by recording substrate concentration-enzyme velocity curves in the presence of different concentrations of test inhibitors. Graphical analysis of the reciprocal Lineweaver-Burk plots showed both increased slopes (decreased V_{max}) and intercepts (higher K_m) at increasing concentration of the inhibitors (**Fig. 4**). This pattern indicated that compounds **9a** and **9b** were both mixed-type inhibitors that could simultaneously bind to CAS and PAS of the AChE enzyme. These kinetic measurements are in good agreement with the results of molecular modeling studies which supports the dual site binding of these compounds. Replots of the slope versus concentration of compounds **9a** and **9b** gave an estimate of the inhibition constant, K_i , of 69 and 102 nM, respectively.

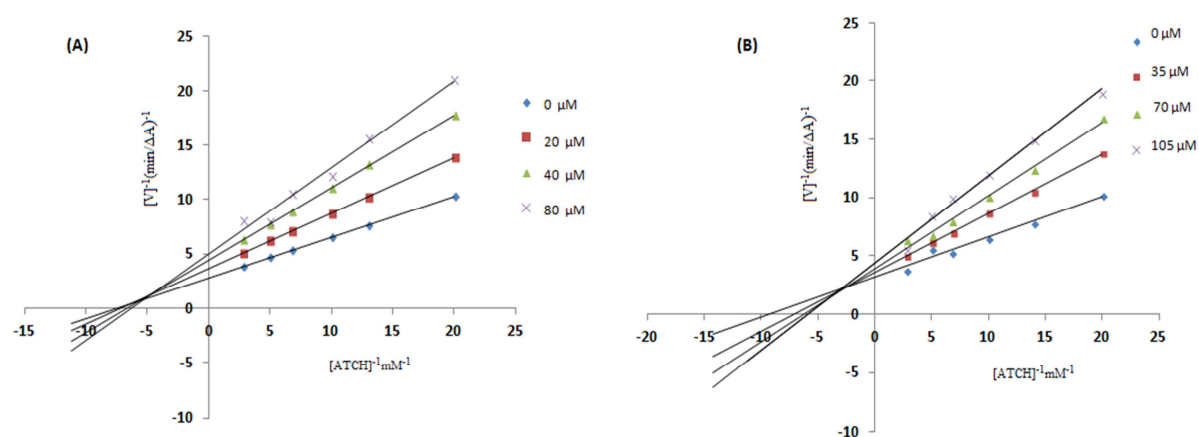


Fig. 4. Kinetic study on the mechanism of EeAChE inhibition by compounds **9a** (A) and **9b** (B). Overlaid Lineweaver-Burk reciprocal plots of EeAChE initial velocity at increasing substrate concentration (0.05-0.50 mM) in the absence of inhibitors and in the presence of **9a** and **9b** are shown.

2.3.3. In vitro antioxidant activity assays

Generation of reactive radical species have been identified as the major contributing factor in AD pathogenesis [23]. Therefore, its reduction is another crucial aspect in designing

multifunctional agents for AD treatment [24][25]. To evaluate the antioxidant activity of new triazine derivatives, the oxygen radical absorbance capacity using fluorescein (ORAC-FL) was employed by following a well-established protocol [26]. Trolox, a water-soluble vitamin E analogue, was used as a standard, and the results were expressed as trolox equivalents (μmol of trolox/ μmol of tested compound), in a relative scale where ORAC (trolox) = 1. As shown in **Table 2**, most of the target compounds demonstrated better antioxidant activity with radical absorbance capacities ranging from 2.91 to 1.04-fold of the trolox value. In general, best results were obtained with derivatives bearing a 4-methoxy substituent at the phenyl ring which seems to be favourable to the compound's overall radical scavenging ability. Especially, compound **9b** exhibited the most potent antioxidant activity within the series with ORAC-FL values of 2.91 trolox equivalents followed by compounds **9a**, **9c**, **3d** and **3g** with 2.15, 1.68, 1.83 and 1.78 trolox equivalents, respectively. However, compounds of tri-substituted triazine series mainly **10d**, **10e** and **10f** showed relatively lower antioxidant activity.

2.3.4. Inhibition of self-mediated $A\beta_{1-42}$ aggregation

The abnormal production and accumulation of misfolded $A\beta$ peptides represents the major triggering factor in the AD pathogenesis. The $A\beta_{1-40}$ and $A\beta_{1-42}$ are the major components of senile plaques found in AD brain. However, $A\beta_{1-42}$ is markedly more fibrillogenic compared to relatively soluble $A\beta_{1-40}$ form [27]. Therefore, prevention of $A\beta_{1-42}$ aggregation is another potential approach for the treatment of AD. With this aim, di and tri-substituted triazine derivatives were selected to assess their ability to inhibit $A\beta_{1-42}$ peptide aggregation by employing thioflavin-T fluorescence assay using curcumin (a known anti-amyloidogenic agent) as the standard. As shown in **Table 3**, most of the tested compounds exhibited significantly higher $A\beta$ aggregation inhibitory activity (1-1.4 folds) at 25 μM compared to the reference

compound curcumin. Compounds **9a-d** of di-substituted triazine series were found to be more effective in blocking the $A\beta_{1-42}$ self-aggregation with inhibition ratio of 75.3% ($IC_{50} = 10.43 \mu M$), 68.5% ($IC_{50} = 11.55 \mu M$), 64.5% ($IC_{50} = 15.89 \mu M$) and 65.8% ($IC_{50} = 13.4 \mu M$), respectively. The trend observed in these set of compounds was found to be similar as observed with cholinesterase inhibition assay. In the screening results of tri-substituted series **10a-f**, the most effective compound was found out to be **10c**, followed by **10f**, **10d** and **10e**, their inhibitory potency are 61.7% ($IC_{50} = 16.29 \mu M$), 58.8% ($IC_{50} = 23.54$), 54.7% ($IC_{50} = 18.31 \mu M$) and 49.3% ($IC_{50} = 25 \mu M$), respectively. On the other hand, compounds **3a-g** gave slightly better inhibitory activity with percentages of inhibition ranging from 65.2% to 46.2% than the compounds of tri-substituted series. Overall, our results revealed that the presence of core triazine moiety is playing a crucial role in binding with beta-amyloid sheets which further prevents $A\beta_{1-42}$ mediated aggregation process.

Table 3. Inhibition of self-induced $A\beta_{1-42}$ aggregation by target compounds 9a-d, 10a-f, 3a-g and reference compound curcumin.

Compounds	$A\beta_{1-42}$ aggregation inhibition (%) ^a	$A\beta_{1-42}$ aggregation IC_{50} (μM) ^b	Compounds	$A\beta_{1-42}$ aggregation inhibition (%) ^a	$A\beta_{1-42}$ aggregation IC_{50} (μM) ^b
9a	75.32 ± 0.34	10.43 ± 0.18	10f	58.80 ± 0.92	23.54 ± 0.99
9b	68.52 ± 0.039	11.55 ± 0.49	3a	65.23 ± 0.44	17.85 ± 0.87
9c	64.53 ± 0.72	15.89 ± 0.88	3b	63.01 ± 0.81	18.55 ± 1.06
9d	65.80 ± 1.03	13.40 ± 1.06	3c	64.77 ± 0.65	20.72 ± 1.18
10a	44.33 ± 0.69	n.t ^c	3d	67.20 ± 0.19	17.60 ± 0.59
10b	22.45 ± 0.52	n.t ^c	3e	46.16 ± 1.22	n.t ^c
10c	61.70 ± 0.75	16.29 ± 1.35	3f	62.52 ± 1.04	18.05 ± 1.36
10d	54.68 ± 0.98	18.31 ± 0.59	3g	60.74 ± 0.78	23.80 ± 0.73
10e	49.33 ± 0.92	25.0 ± 0.81	Curcumin	54.32 ± 0.95	22.51 ± 0.89

^aInhibition of self-induced A β ₁₋₄₂ aggregation (25 μ M) by tested inhibitors at 25 μ M by thioflavin-T based fluorescence method (means \pm SD of three experiments).

^bThe concentration (μ M) required for 50% inhibition was determined from dose-response curves. Data are expressed as means \pm SD of three independent experiments.

^cn.t. means not tested

2.3.5. Effect on A β β -sheet formation by compounds **9a** and **9b**

A β fibril formation has been correlated with secondary structure transitioning from disordered random structure to ordered β -sheet-rich conformation [28][29]. On this premise, finding small molecules that ubiquitously prevent the conformational transition from initial random coil or α -helix into β -sheet seems to be intriguing for AD therapeutic development. In order to elucidate the structural details of the interactions between A β ₁₋₄₂ and the triazine derivatives (**9a** and **9b**), CD spectroscopy was utilized as a means to obtain information about the mechanism of action of these inhibitors in preventing conformational changes in A β ₁₋₄₂ peptide. As shown in **Fig. 6A**, the CD spectrum of A β ₁₋₄₂ monomer did not exhibit any spectral feature of α -helix and β -sheet, but showed characteristic features of dominantly unordered structure. The spectra recorded after the incubation period of 12 h indicated fall of unstructured conformation content and a small rise in α -helix (**Fig. 6B**). The spectra recorded in the presence of **9a** and **9b** co-incubated with peptide for 12 h assumes shapes closer to those characteristic for the α -helix conformation with very low β -sheet and random structures (**Fig. 6B**). The representative CD spectra of aggregated A β ₁₋₄₂ after 24 h exhibited a characteristic pattern of β -sheet conformation with absorption minimum around 217 nm (**Fig. 6C**), which indicate that disordered A β ₁₋₄₂ monomers aggregated into β -sheet rich fibrillar aggregates after the incubation. However, the treatment of **9a** and **9b** to A β ₁₋₄₂ peptide permitted different structural transitions compared with those observed when A β ₁₋₄₂ was incubated alone (**Fig. 6C**). Intriguingly, CD spectrum clearly assessed that these compounds caused a decrease in the CD ellipticity measured at 217 nm,

indicating their preventing effect on A β from adopting a β -sheet rich conformation. These results revealed that test compounds could reduce the β -sheet structure formation thereby hampering further aggregation into mature fibrils.

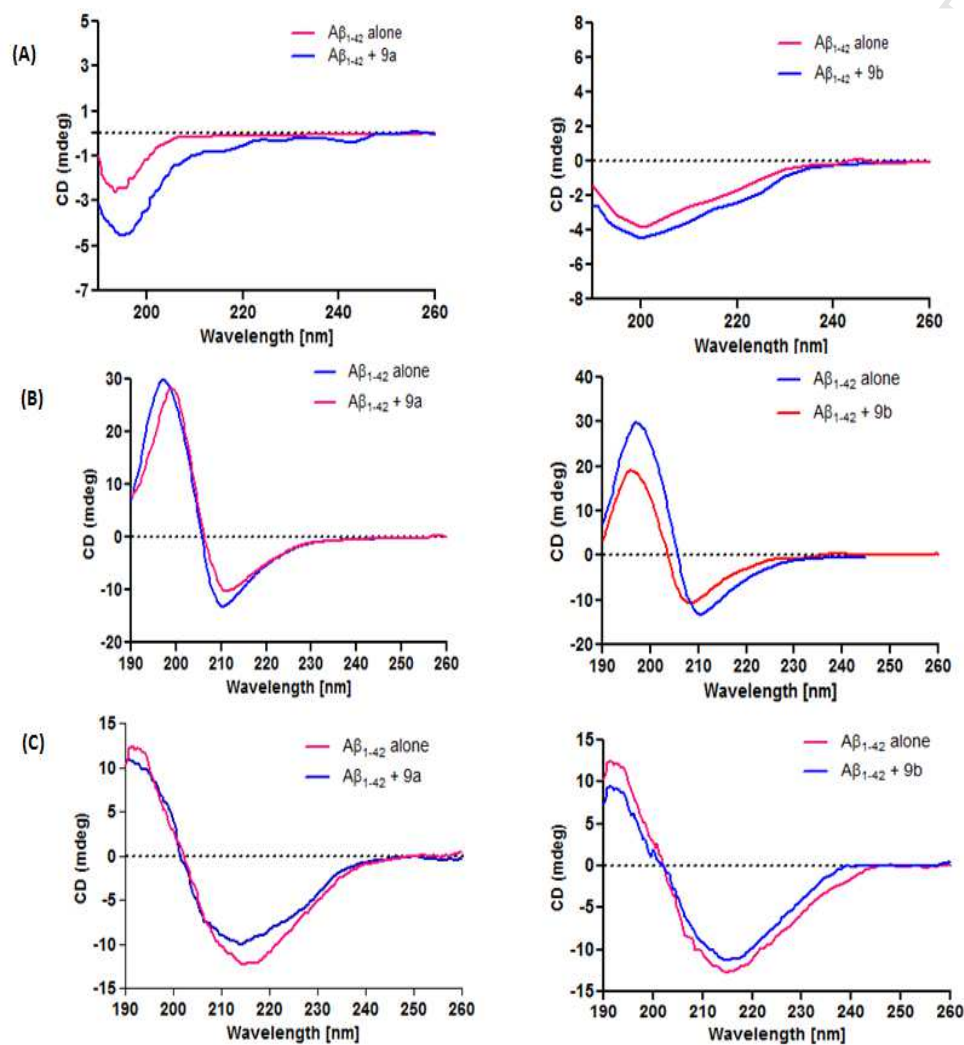


Fig.5. CD spectroscopy of A β ₁₋₄₂ alone or with compounds 9a and 9b incubated for 0 h (A), 12 h (B) and 24 h (C). A β ₁₋₄₂ (20 μ M) was incubated either alone in 20 mM sodium phosphate buffer (pH 7.4) at 37 $^{\circ}$ C, or in the presence of 20 μ M 9a and 9b.

2.3.6. Inhibition of A β ₁₋₄₂ fibril formation monitored by transmission electron microscopy TEM

Next, TEM study was employed in order to monitor and probed the degree of A β aggregation after compound (**9a** and **9b**) treatment. At 0 h time point, there was no aggregation

in the samples containing $A\beta_{1-42}$ with (Fig. 6A) or without compounds (data not shown). However, after 24 h of incubation at 37 °C, the sample of $A\beta_{1-42}$ alone had mostly aggregated into dense, mature and bulky amyloid fibrils (Fig. 6B). In contrast, only fewer and shorter aggregates were visible in the electron micrographs of $A\beta_{1-42}$ samples after incubation with compounds 9a and 9b (Fig. 6D and E) under the same experimental conditions as compared to standard curcumin (Fig. 6C). The TEM results were in agreement with the results of ThT binding studies, which further proved that these compounds could effectively inhibit and slow down the rate of $A\beta_{1-42}$ fibrils formation *in vitro*.

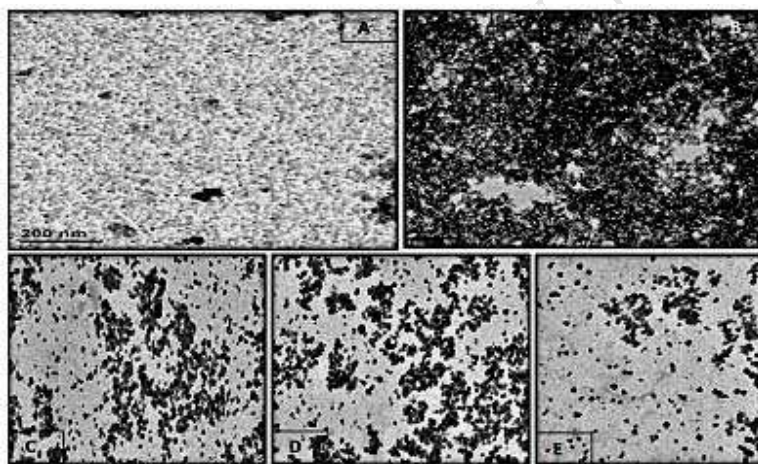


Fig. 6. TEM image analysis of $A\beta_{1-42}$ aggregation in the presence of 9a and 9b. (A) $A\beta_{1-42}$ (25 μ M), 0 h. (B) $A\beta_{1-42}$ alone (25 μ M) was incubated at 37 °C for 24 h. (C) $A\beta_{1-42}$ (25 μ M) and curcumin (25 μ M) were incubated at 37 °C for 24 h. (D) $A\beta_{1-42}$ (25 μ M) and 9a (25 μ M) were incubated at 37 °C for 24 h. (E) $A\beta_{1-42}$ (25 μ M) and 9b (25 μ M) were incubated at 37 °C for 24 h.

2.3.7. Inhibition of AChE-induced $A\beta_{1-42}$ aggregation

The discovery that AChE plays additional roles, besides its "classical" function in terminating synaptic transmission, has gained further attention in its role as target for AD therapy. In particular, PAS of AChE has been identified as a site promoting non-cholinergic functions by accelerating the assembly of $A\beta$ fibrils that contribute towards the neurotoxic cascade of AD [30][31][32]. On this premise, novel classes of AChE inhibitors targeting PAS

have emerged as promising disease-modifying AD drug candidates. Thus, the triazine derivatives (**9a** and **9b**) showing best AChE inhibitory potency were further selected to assess their inhibitory activity on the AChE-induced $A\beta_{1-42}$ peptide aggregation by employing the same ThT-based fluorometric assay. In particular, test compounds were screened at a single concentration and compared with reference compound donepezil. After 24 h of incubation, there observed a remarkable increase in the intensity of ThT fluorescence signal from co-incubated samples of AChE- $A\beta$ which clearly indicated acceleration of $A\beta$ fibrillogenesis by AChE. This increase fluorescence yield was significantly reduced in the presence of compounds **9a** and **9b** (Fig. 7) by ~45% and ~58%, respectively, which was higher than that of donepezil (22.8%). The results of ThT assay further confirmed the dual mode of inhibition and suggested that targeted compounds **9a** and **9b** may have a potential disease-modifying role in AD therapy.

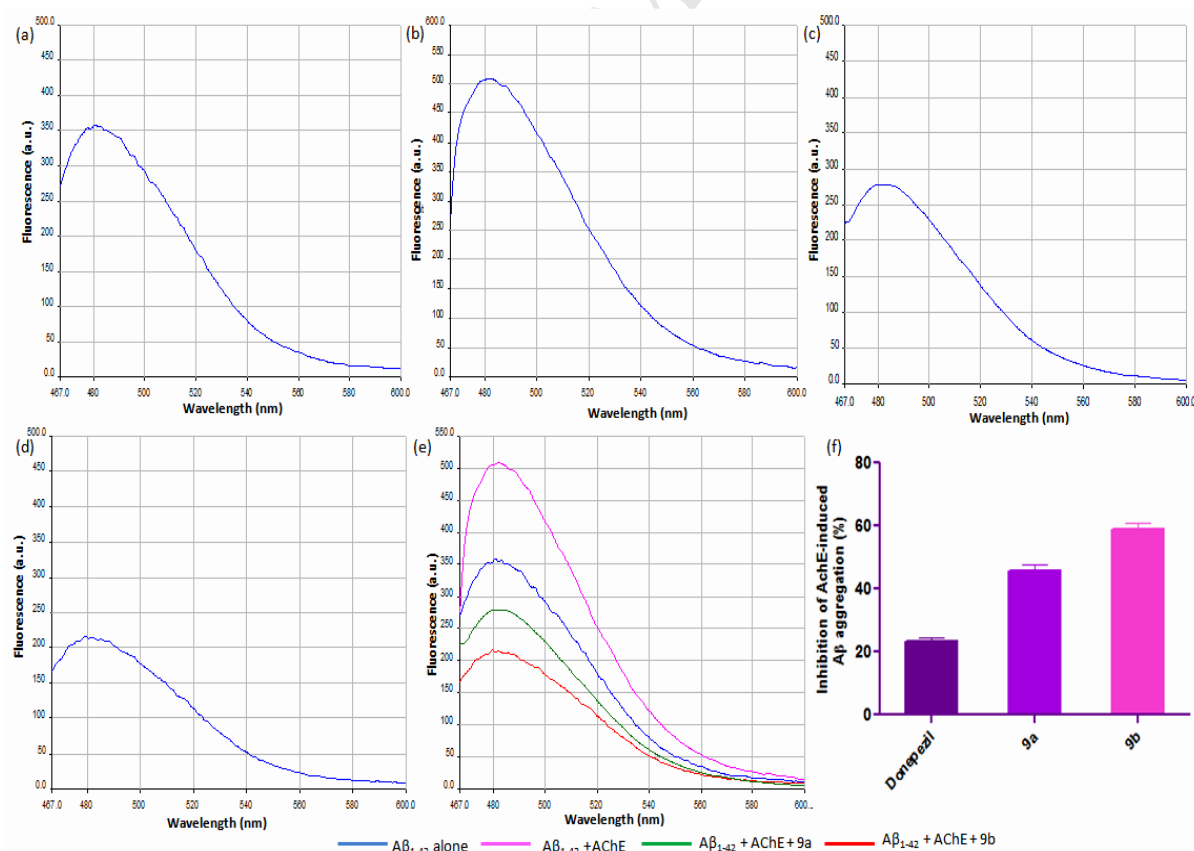


Fig. 7. ThT emission fluorescence spectra (range 450-600 nm) in the absence of AChE (a) $A\beta_{1-42}$ alone, and in the presence of (b) $A\beta_{1-42}$ +AChE, (c) **9a**+ $A\beta_{1-42}$ +AChE, (d) **9b**+ $A\beta_{1-42}$ +AChE, (e) Overlay of ThT emission fluorescence spectra, (f) The inhibitory activity of test compounds to AChE-induced $A\beta_{1-42}$ aggregation in ThT binding assay. The concentration of $A\beta_{1-42}$ was 25 μ M, and the concentration ratio of $A\beta_{1-42}$, AChE, compound was 100:1:100.

2.3.8. Metal-chelating properties of compound **9a** and **9b**

The ability of **9a** and **9b** to chelate biometals such as Cu^{2+} , Zn^{2+} and Fe^{2+} was studied by UV-vis spectroscopy [33]. Upon the addition of $CuSO_4$, a red shift in the maximum absorption from 208 nm to 214 nm and 228 nm to 238 nm occurred, indicating the formation of a **9a**- Cu^{2+} complex (**Fig. 8a**). The maximum absorption at 228 nm exhibited a significant shift when $FeSO_4$ and $ZnCl_2$ was added, suggesting that **9a** binds to Fe^{2+} and Zn^{2+} . Interestingly, when the same experiment was performed with compound **9b**, the maximum absorption at 228 nm was shifted to 234 or 236 nm, respectively, suggesting complexes formation of **9b**- Fe^{2+} and **9b**- Zn^{2+} , respectively (**Fig. 8b**).

The stoichiometry of the **9a**- Cu^{2+} complex was investigated using the molar ratio method, by preparing solutions of compound **9a** with increasing amounts of $CuSO_4$. The UV spectra were used to obtain the absorbance of the complex of **9a** and $CuSO_4$ at different concentrations at 238 nm. As indicated in **Fig. 8c**, the absorbance linearly increased at first. When the mole fraction of Cu^{2+} to **9a** was more than 0.9, the absorbance tended to be stable. Therefore, two straight lines were drawn with the intersection point at a mole fraction of 0.9, which implied a 1:1 stoichiometry for the **9a**- Cu^{2+} complex. The stoichiometric ratio of the **9b**- Cu^{2+} complex was determined at 236 nm (**Fig. 8d**). The mole fraction was found to be 0.96, suggesting a 1:1 stoichiometry for the complex. These observations reflect the ability of test compounds to

chelate biometals, and therefore could serve as potential metal chelators for AD therapy.

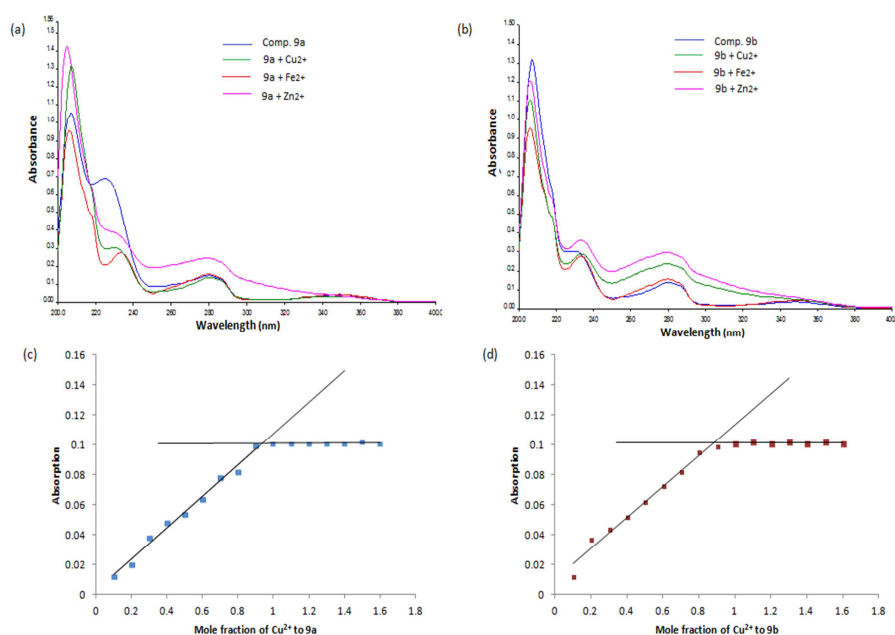


Fig. 8. (a) UV spectrum of compound 9a (50 μM) alone and in the presence of CuSO₄ (50 μM), FeSO₄ (50 μM) and ZnCl₂ (50 μM). (b) UV spectrum of compound 9b (50 μM) alone and in the presence of CuSO₄ (50 μM), FeSO₄ (50 μM) and ZnCl₂ (50 μM). (c) Determination of the stoichiometry of complex 9a-Cu(II) by Job's method. (d) Determination of the stoichiometry of complex 9b-Cu(II) by Job's method.

2.3.9. Effect of compounds 9a and 9b on Cu²⁺-induced Aβ₁₋₄₂ aggregation

To investigate the ability of the triazine derivatives to inhibit metal-induced Aβ aggregation, we studied the effect of most potent compounds **9a** and **9b** on metal-induced Aβ₁₋₄₂ aggregation by ThT fluorescence assay. Curcumin was used as reference compound. As shown in **Fig. 9**, the fluorescence of Aβ treated with Cu²⁺ is 156.4 % that of Aβ alone (100 %), which demonstrates that Cu²⁺ accelerates Aβ aggregation. On the contrary, the fluorescence of Aβ treated with Cu²⁺ and the tested compounds decreased dramatically (**9a**, 69.7 % inhibition of Cu²⁺-induced Aβ aggregation; **9b**, 66.6 % inhibition and curcumin, 60.28 % inhibition) at a concentration ratio of 1:1:2 [Aβ (25 μM):Cu²⁺ (25 μM):Inhibitor (50 μM)]. These results

suggested that our compounds could inhibit Cu^{2+} -induced $\text{A}\beta_{1-42}$ aggregation noticeably through chelating with Cu^{2+} ions.

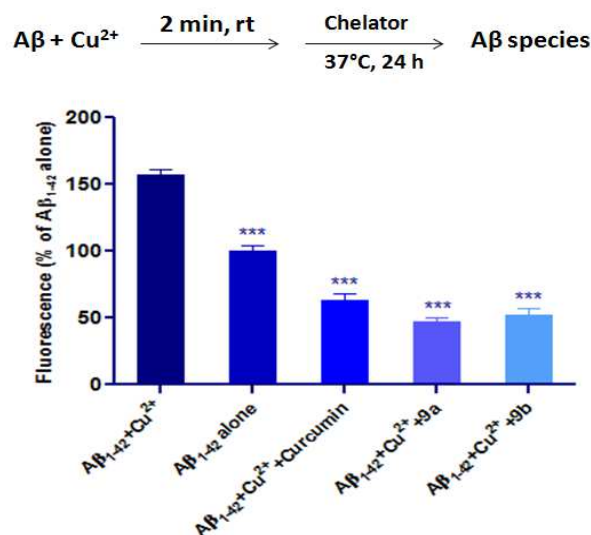


Fig. 9. ThT binding assay for Cu^{2+} -induced $\text{A}\beta$ aggregation, and test compound induced $\text{A}\beta$ disaggregation. Values are reported as the mean \pm SD of three independent experiments. Statistically significant differences from $\text{A}\beta_{1-42} + \text{Cu}^{2+}$ were analyzed by ANOVA: *** $p < 0.001$.

2.3.10. Inhibition of compounds **9a** and **9b** on Cu^{2+} -induced $\text{A}\beta_{1-42}$ aggregation monitored by TEM

To further confirm the ability of compounds **9a** and **9b** to inhibit Cu^{2+} -mediated $\text{A}\beta_{1-42}$ aggregation, TEM analysis was performed. As depicted in **Fig. 10C**, Cu^{2+} (25 μM) could accelerate the aggregation of $\text{A}\beta_{1-42}$ (25 μM) which was evident by the presence of denser fibrillar aggregates compared with $\text{A}\beta_{1-42}$ alone samples (**Fig. 10B**) under the same experimental conditions. However, there observed a alteration in the metal-triggered $\text{A}\beta$ aggregation upon **9a** and **9b** (50 μM each) addition as indicated by the presence of only fewer $\text{A}\beta$ aggregates which clearly suggested that these compounds provided considerable disaggregation effect (**Fig. 10E** and **10F**). The observations of TEM are consistent with ThT binding assay results which

suggested that metal chelation by these compounds may be one of the driving forces in altering the structural organization of A β aggregates.

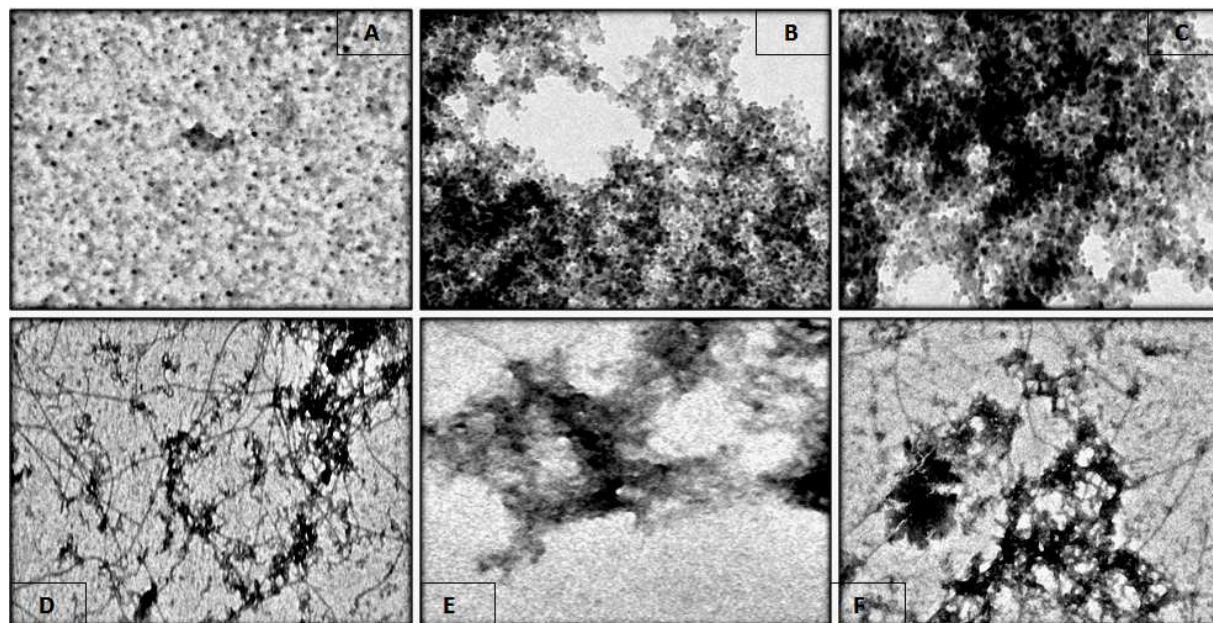


Fig. 10. TEM images for Cu²⁺-induced A β aggregation and test compound induced A β disaggregation. ([A β ₁₋₄₂] = 25 μ M, [Cu²⁺] = 25 μ M, [9a] = 50 μ M, [9b] = 50 μ M, [curcumin] = 50 μ M, 37 °C, 24 h; (A) A β ₁₋₄₂, 0 h; (B) A β ₁₋₄₂ alone; (C) A β ₁₋₄₂ + Cu²⁺, (D) A β ₁₋₄₂ + Cu²⁺ + 9a; (E) A β ₁₋₄₂ + Cu²⁺ + 9b; (F) A β ₁₋₄₂ + Cu²⁺ + curcumin).

2.3.11. Bioavailability and ADME parameters screening for drug likeness

The assessment of pharmacokinetic properties is one of the critical stages in the drug development process. *In silico* ADMET analysis can be used to check the lead candidates for their plausible drug likeness and bioavailability. The computational tool QikProp, v. 3.5 available in Schrödinger software has been used to study the pharmacokinetic profile of the targeted compounds [34]. A few significant indicators of their pharmacokinetic profiles were considered with special emphasis on the requirements of a CNS active drug (**Table S1, Supplementary material**). Our results indicated that most of the compounds showed drug like characteristics based on Lipinski's rule of five (mol_MW < 500, QPlogPo/w < 5, donorHB \leq 5, acceptHB \leq 10). Based on the predicted values for QPlogBB and CNS activity, all compounds

might be able to penetrate into the CNS. Generally, drugs aimed at the CNS tends to have lower polar surface area (PSA) usually between 60 and 70 Å² [35]. The calculated theoretical PSA values for all compounds may support their ability to penetrate the blood-brain barrier. The distribution of the compound in the human body depends on factors such as blood-brain barrier (QPLog BB), permeability such as apparent Caco-2 permeability (QPPCaco), apparent MDCK cell permeability (QPPMDCK), volume of distribution and plasma protein binding (QPLogKhsa for Serum protein binding). All of these compounds exhibited high permeability for both *in vitro* Caco-2 cells and *in vitro* MDCK cells. Moreover, all compounds displayed good oral absorption. The predicted QPlogKhsa values of all compounds were found to be within acceptable range which indicates their strong binding with plasma protein. The predicted ADME properties revealed that these compounds possess appropriate pharmacokinetic profiles required to penetrate BBB and therefore, could be considered as good candidate for drug development.

2.3.12. Toxicity prediction

Toxicity predictor (TOPKAT module of Accelrys Discovery Studio 4.0) computes a probable value of toxicity for a submitted chemical structure using quantitative structure-activity relationship (QSTR) equation and locates fragments within the compound that indicate a potential threat to toxicity risk. Parameters for toxicity risk such as carcinogenicity, mutagenicity, skin irritancy, ocular irritancy, aerobic biodegradability and developmental toxicity potential etc., were observed for synthesized compounds **9a-b**, **10a-f** and **3a-g**. The results of toxicity risk for triazine derivatives showed moderate to good drug score. In general, toxicity screening results of TOPKAT for USFDA and NTP predicted rodent carcinogenicity, Ames mutagenicity, developmental toxicity potential, aerobic biodegradability, ocular irritancy and skin irritancy showed positive response for most of the triazine derivatives (**Table S2**,

Supporting file). Overall, these results indicated that for all the default parameters, computed probabilities of toxicity were low to intermediate for most of the compounds.

3. Conclusion

In summary, a series of new class of triazolopyrimidine-triazine hybrids were designed, synthesized and evaluated as multifunctional anti-Alzheimer agents. These compounds were found to have potential cholinesterase inhibitory activity and high selectivity for AChE over BuChE by approximately 28 fold. Persuasive radical scavenging ability of the synthesized compounds was also recorded. Di-substituted triazine-triazolopyrimidine derivatives **9a-d** showed better AChE inhibitory activity than the corresponding tri-substituted triazine-triazolopyrimidine derivatives **10a-f**. Compounds **9a** and **9b** showed best results among the series for the inhibition of AChE with IC_{50} values 0.065 and 0.092 μ M respectively. Significant anti- $A\beta_{1-42}$ aggregation potency of the compounds was also observed. Dual binding affinity of these compounds was revealed by molecular modelling and kinetic studies which figured out that these compounds act as mixed-type inhibitors due to their affinity towards both the CAS and PAS of AChE. Persuasive radical scavenging ability of the synthesized compounds was also recorded. Significant anti- $A\beta_{1-42}$ aggregation potency of the compounds was also observed. In addition, **9a** and **9b** showed a balanced multitargeted profile with significant inhibition of self-induced and AChE-mediated $A\beta$ aggregation as evidenced through different biophysical experiments. These compounds also possessed the prospective property of acting as potential antioxidants, biometal chelators and exhibited better Cu^{2+} -induced $A\beta_{1-42}$ aggregation inhibitory potency. Drug-like properties of these compounds were proven using the theoretic ADME analysis. Altogether, the multitargeted profile of the triazine-triazolopyrimidine derivatives

elucidated that these derivatives can be considered very capable lead compounds for anti-AD therapy.

4. Experimental

4.1. Chemistry

The reagents and solvents purchased were of the highest commercial quality and used without further purification. All the moisture sensitive reactions were performed under nitrogen (N_2) medium. The reactions were monitored by thin layer chromatography (TLC) on 0.25 mm silica gel-coated plates (Merck 60 F254, Germany) using HPLC grade solvents. Separation and purification of all the synthesized compounds were done by column chromatography using silica gel 60-120 mesh, Merck. Melting points were determined on Veego melting point instrument (REC-22038 A2) and were uncorrected. Structure elucidations of the newly synthesized compounds were attained by the aid of elemental analysis (Elemental Vario analyser). 1H NMR and ^{13}C NMR spectra were recorded on a Bruker Avance 300 and 400 MHz spectrometer in $CDCl_3$ or $DMSO-d_6$ as a solvent with TMS as the internal standard. The chemical shifts (δ) were reported in ppm and coupling constants (J) were given in Hz. ESI-MS were determined on Applied Biosystem (ABSCIEX-2000 Triple quad) spectrometer. The spectra of all synthesized compounds are provided in the supporting file of the article.

4.1.1. General procedure for the synthesis of mono-substituted triazine [2 (a-e)]

Synthesis of mono-substituted triazine compound is shown in **Scheme 1**. Cyanuric chloride (5.03 g; 1.1 equiv) was dissolved in anhydrous THF at $-10\text{ }^\circ\text{C}$ and K_2CO_3 (3.43 g; 1 equiv) was added. Appropriate aromatic amines (4 g; 1.0 equiv) were dissolved in THF and were added drop wise to the reaction mixture for half an hour with constant stirring. The progress of the reaction was monitored by thin layer chromatography. After the completion of the reaction,

the reaction mixture was dried with a rotatory evaporator. The reaction was quenched with water and extracted with ethyl acetate (2×50 mL). The organic layer was washed with brine solution, dried over Na₂SO₄ and evaporated at reduced pressure to get the crude products. The crude products were purified by silica gel column chromatography eluted with petroleum ether and EtOAc (2–3%) to give the pure compounds 2 (a-e), which was used for the next step reaction.

4.1.2. General procedure for the synthesis of di-substituted triazine [3 (a-g)]

Synthesis of di-substituted triazine is also depicted in **Scheme 1**. A solution of appropriate aromatic/ aliphatic amine (0.87 g; 1.0 equiv) in THF (5 mL) was added drop wise to the stirred solution of mono-substituted triazine (2.5 g; 1.0 equiv) and K₂CO₃ (1.1 g; 1.0 equiv) in anhydrous DMF (5 mL) at 0 °C. Then the reaction mixture was continued to stir at room temperature for 6–12 hrs. The progress of the reaction was monitored by thin layer chromatography. After the completion of the reaction, the reaction mixture was quenched with water and extracted with ethyl acetate (3×50 mL). The organic layer was washed with brine solution and then dried over Na₂SO₄ and evaporated to dryness. The compounds 3 (a-g) were also purified by column chromatography eluted with petroleum ether and EtOAc (6–8%) and were used for the further reactions.

Representative procedure for the synthesis of triazolopyrimidine based compound:

4.1.3. General procedure for the preparation of compound 6

A mixture of 3-amino-1,2,4-triazole (1.0 equiv) and ethyl acetoacetate (1.0 equiv) was heated under reflux in 10 mL of acetic acid for 4-5 hrs. After the reaction mixture cooled to room temperature, the solid precipitate formed was filtered, washed with acetic acid followed by ethanol, and dried under vacuum to get the desired product with 45-55% yield.

5-Methyl-[1,2,4]triazolo[1,5-a]pyrimidin-7-ol (6)

White solid crystal; yield: 55%; mp: 287 °C; ESI-MS: $m/z = 151.1 [M+H]^+$; 1H NMR (300 MHz, DMSO- d_6): δ 11.52 (s, 1H, -OH), 8.15 (s, 1H, Triazolopyrimidine- H_b), 5.82 (s, 1H, Triazolopyrimidine- H_a), 2.30 (s, 3H, Triazolopyrimidine- CH_3).

4.1.4. General procedure for the preparation of compound 7

The formed 5-Methyl-[1,2,4] triazolo [1,5- a] Pyrimidin-7-ol (1.0 equiv) was added to 2.75 mL (3.0 equiv) of phosphorous oxychloride and heated under reflux for 90 min in a round bottom flask. Excess phosphorous oxychloride was removed under reduced pressure on a rotatory evaporator, and the residue was triturated with ice water. The product was extracted from the aqueous mixture with CH_2Cl_2 , organic layer was dried over sodium sulphate, evaporated at reduced pressure, and purified by column chromatography using 60% EtOAc/hexane.

7-Chloro-5-methyl-[1,2,4]triazolo[1,5- a]pyrimidine (7)

White-yellow solid; Yield: 55%; mp: 150 °C; ESI-MS: $m/z = 169.1 [M+H]^+$; 1H NMR (300 MHz, $CDCl_3$): δ 8.50 (s, 1H, Triazolopyrimidine- H_b), 7.15 (s, 1H, Triazolopyrimidine- H_a), 2.75 (s, 3H, Triazolopyrimidine- CH_3).

4.1.5. General procedure for the preparation of compound 8

A mixture of appropriate compound 7 (1.0 equiv), piperazine, (1.0 equiv) and K_2CO_3 (1.2 equiv) in 1,4-dioxane was reflux at 100 °C for 3 hrs. The reaction mixture was cooled to room temperature, filter and washed with 1,4-dioxane. The filtrate was concentrated and dried by vacuum.

5-methyl-7-(piperazin-1-yl)-[1,2,4]triazolo[1,5- a]pyrimidine (8)

Yellowish solid; Yield: 70%; 1H NMR (400 MHz, $CDCl_3$) δ 8.23 (s, 1H, Triazolopyrimidine- H_b), 6.09 (s, 1H, Triazolopyrimidine- H_a), 3.73 (4H, Piperazine), 3.63 (s, 1H,

-NH), 3.05 (4H, Piperazine), 2.51 (s, 3H, Triazolopyrimidine-CH₃); ¹³C NMR (100 MHz, CDCl₃) δ 164.7, 157.2, 153.9, 150.7, 94.5, 49.2, 45.8, 25.2.

4.1.6. General procedure for the synthesis of di-substituted triazine triazolopyrimidine piperazine 9 (a-d).

A mixture of compound **8** (1.2 equiv), compound **2** (1.0 equiv) and K₂CO₃ (1.2 equiv) in 1,4-dioxane was stirred at room temperature for 12-16 hrs. After the completion of reaction monitored by TLC, the reaction mixture was filtered and washed with 1,4-dioxane. The filtrate was vacuum dried and obtained the crude product which was purified by column chromatography by 70-80% EtOAc/ Hexane to obtain the pure di-substituted triazine-triazolopyrimidine piperazine **9** (a-d) compounds.

4-chloro-6-(4-(5-methyl-[1,2,4]triazolo[1,5-a]pyrimidin-7-yl)piperazin-1-yl)-N-(3-(trifluoromethyl)phenyl)-1,3,5-triazin-2-amine 9 (a).

White solid; yield: 73%; mp: 210-220 °C; ESI-MS: m/z = 491.2 [M+H]⁺; ¹H NMR (400 MHz, DMSO-*d*₆) δ 10.47 (s, 1H, -NH₅), 8.43 (s, 1H, Triazolopyrimidine-H_b), 8.14 (s, 1H, Ar-H₄), 7.84 (d, *J* = 8.4 Hz, 1H, Ar-H₁), 7.54 (1H, Ar-H₂), 7.37 (d, *J* = 8.0 Hz, 1H, Ar-H₃), 6.60 (s, 1H, Triazolopyrimidine-H_a), 3.38 (s, 8H, Piperazine), 2.46 (s, 3H, Triazolopyrimidine-CH₃). ¹³C NMR (100 MHz, DMSO-*d*₆) δ 164.78, 157.07, 154.43, 149.93, 140.02, 132.13, 130.51, 129.72, 127.80, 126.02, 124.26, 123.31, 119.84, 116.92, 95.42, 47.58, 43.08, 25.98. Anal. Calcd. for C₂₀H₁₈ClF₃N₁₀: C, 48.94; H, 3.70; N, 28.53; Found: C, 49.21; H, 3.89; N, 28.12.

4-chloro-N-(4-methoxyphenyl)-6-(4-(5-methyl-[1,2,4]triazolo[1,5-a]pyrimidin-7-yl)piperazin-1-yl)-1,3,5-triazin-2-amine 9 (b).

Off white solid; yield: 80%; mp: 230-240 °C; ESI-MS: m/z = 453.2 [M+H]⁺; ¹H NMR (400 MHz, DMSO-*d*₆) δ 10.03 (s, 1H, -NH₅), 8.44 (s, 1H, Triazolopyrimidine-H_b), 7.53 (d, *J* =

8.4 Hz, 2H, Ar-H_{1,4}), 6.89 (d, $J = 8.8$ Hz, 2H, Ar-H_{2,3}), 6.61 (s, 1H, Triazolopyrimidine-H_a), 3.89 (s, 3H, Anisidine-CH₃), 3.70 (s, 8H, Piperazine), 2.46 (s, 3H, Triazolopyrimidine-CH₃). Anal. Calcd. for C₂₀H₂₁ClN₁₀O: C, 53.04; H, 4.67; N, 30.93; Found: C, 53.48; H, 4.83; N, 31.22.

4-chloro-N-(4-fluorophenyl-6-(4-(5-methyl-[1,2,4]triazolo[1,5-a]pyrimidin-7-yl)piperazin-1-yl)-1,3,5-triazin-2-amine 9 (c).

White solid; yield: 75%; mp: 220-230 °C; ESI-MS: $m/z = 441.2$ [M+H]⁺; ¹H NMR (400 MHz, DMSO-*d*₆) δ 10.20 (s, 1H, -NH₅), 8.43 (s, 1H, Triazolopyrimidine-H_b), 7.63 (s, 2H, Ar-H_{1,4}), 7.15 (2H, Ar-H_{2,3}), 6.59 (s, 1H, Triazolopyrimidine-H_a), 3.93 (s, 8H, Piperazine), 2.46 (s, 3H, Triazolopyrimidine-CH₃). ¹³C NMR (100 MHz, DMSO-*d*₆) δ 164.73, 163.81, 160.96, 159.77, 157.12, 154.45, 153.56, 149.92, 135.48, 122.55, 115.95, 115.73, 105.54, 95.35, 47.53, 43.07, 25.11. Anal. Calcd. for C₁₉H₁₈ClFN₁₀: C, 51.76; H, 4.12; N, 31.77; Found: C, 51.83; H, 4.73; N, 31.52.

4-chloro-N-(2-fluorophenyl-6-(4-(5-methyl-[1,2,4]triazolo[1,5-a]pyrimidin-7-yl)piperazin-1-yl)-1,3,5-triazin-2-amine 9 (d).

White solid; yield: 70%; mp: 230-240 °C; ESI-MS: $m/z = 441.2$ [M+H]⁺; ¹H NMR (400 MHz, CDCl₃) δ 8.34 (s, 1H, Triazolopyrimidine-H_b), 8.19 (s, 1H, -NH₅), 7.31 (2H, Ar-H_{2,3}), 7.16 (d, $J = 8.4$ Hz, 1H, Ar-H₁), 7.09 (d, $J = 7.2$ Hz, 1H, Ar-H₄), 6.19 (s, 1H, Triazolopyrimidine-H_a), 3.92 (4H, Piperazine), 3.80 (4H, Piperazine), 2.61 (s, 3H, Triazolopyrimidine -CH₃). ¹³C NMR (100 MHz, CDCl₃) δ 165.30, 164.01, 154.55, 152.20, 150.13, 149.53, 134.02, 129.51, 126.12, 124.43, 122.41, 122.14, 117.20, 95.03, 47.62, 43.04, 25.42. Anal. Calcd. for C₁₉H₁₈ClFN₁₀: C, 51.76; H, 4.12; N, 31.77; Found: C, 51.83; H, 4.73; N, 31.52.

4.1.7. General procedure for the synthesis of tri-substituted triazine triazolopyrimidine piperazine 10 (a-e).

A mixture of compound **8** (1.2 equiv), compound **3** (1.0 equiv) and K_2CO_3 (1.2 equiv) in 1,4-dioxane was reflux at 100 °C for 12-16 hrs. After the completion of reaction monitored by TLC, the reaction mixture was filtered and washed with 1,4-dioxane. The filtrate was vacuum dried and obtained the crude product. The obtained crude was further purified by column chromatography by 75-85% EtOAc/ Hexane to obtain the pure tri-substituted triazine triazolopyrimidine piperazine **10** (a-e) compounds.

N2-cyclopropyl-6-(4-(5-methyl-[1,2,4]triazolo[1,5-a]pyrimidin-7-yl)piperazin-1-yl)-N4-(3-(trifluoromethyl)phenyl)-1,3,5-triazine-2,4diamine 10 (a).

White solid; yield: 65%; mp: 190-200 °C; ESI-MS: $m/z = 512.0 [M+H]^+$; 1H NMR. 1H NMR (300 MHz, $CDCl_3$) δ 8.34 (s, 2H, $-NH_{8,9}$), 7.52 (d, $J = 8.1$ Hz, 2H, Ar- $H_{1,3}$), 7.39 (2H, Triazolopyrimidine- H_b and Ar- H_2), 7.27 (2H, Ar- H_4 and Triazolopyrimidine- H_a), 6.19 (s, 1H, Ar- H_5), 5.48 (s, 2H, Cyclopropyl- H_6), 5.08 (s, 2H, Cyclopropyl- H_7), 4.07 (s, 4H, Piperazine), 3.86 (s, 4H, Piperazine), 2.60 (s, 3H, Triazolopyrimidine- CH_3). ^{13}C NMR (75 MHz, $CDCl_3$) δ 175.92, 165.08, 164.77, 157.12, 154.22, 150.16, 139.88, 131.16, 130.74, 129.09, 126.01, 122.41, 118.96, 116.84, 94.65, 47.82, 42.64, 25.17, 23.46, 21.32, 7.17. Anal. Calcd. for $C_{23}H_{24}F_3N_{11}$: C, 54.01; H, 4.73; N, 30.12; Found: C, 54.35; H, 4.91; N, 30.04.

6-(4-(5-methyl-[1,2,4]triazolo[1,5-a]pyrimidin-7-yl)piperazin-1-yl)-N2-(p-tolyl)-N4-(3-(trifluoromethyl)phenyl)-1,3,5-triazine-2,4diamine 10 (b).

Light brown solid; yield: 71%; mp: 240-250 °C; ESI-MS: $m/z = 562.2 [M+H]^+$; 1H NMR (300 MHz, $DMSO-d_6$) δ 9.34 (s, 1H, $-NH_{10}$), 9.00 (s, 1H, $-NH_9$), 8.26 (s, 1H, Triazolopyrimidine- H_b), 8.00 (s, 1H, Ar- H_4), 7.82 (d, $J = 6.3$ Hz, 1H, Ar- H_1), 7.40 (d, $J = 7.8$ Hz, 2H, Ar- $H_{6,7}$), 7.30 (1H, Ar- H_2), 7.09 (d, $J = 7.8$ Hz, 1H, Ar- H_3), 6.90 (d, $J = 8.1$ Hz, 2H, Ar-

H_{5,8}), 6.43 (s, 1H, Triazolopyrimidine-H_a), 3.76 (8H, Piperazine), 3.11 (s, 3H, Toulidine-CH₃), 2.30 (s, 3H, Triazolopyrimidine-CH₃). ¹³C NMR (75 MHz, DMSO-*d*₆) δ 164.99, 164.54, 156.99, 154.27, 150.03, 141.46, 137.67, 131.45, 129.94, 129.49, 129.28, 126.58, 123.70, 120.89, 118.25, 116.32, 95.27, 47.79, 42.70, 24.95, 20.85. Anal. Calcd. for C₂₇H₂₆F₃N₁₁: C, 57.75; H, 4.67; N, 27.44; Found: C, 57.93; H, 4.79; N, 27.23.

N2-(3-chloro-4-fluorophenyl)-6-(4-(5-methyl-[1,2,4]triazolo[1,5-a]pyrimidin-7-yl)piperazin-1-yl)-N4-(3-(trifluoromethyl)phenyl)-1,3,5-triazine-2,4diamine 10 (c).

White solid; yield: 76%; mp: 260-270 °C; ESI-MS: *m/z* = 600.2 [M+H]⁺; ¹H NMR (300 MHz, DMSO-*d*₆) δ 9.67 (s, 1H, -NH₉), 9.51 (s, 1H, -NH₈), 8.48 (s, 1H, Triazolopyrimidine-H_b), 8.16 (s, 1H, Ar-H₄), 8.00 (d, *J* = 4.5 Hz, 2H, Ar-H_{1,2}), 7.68 (s, 1H, Ar-H₃), 7.54 (1H, Ar-H₆), 7.32 (d, *J* = 7.8 Hz, 2H, Ar-H_{5,7}), 6.65 (s, 1H, Triazolopyrimidine-H_a), 3.97 (8H, Piperazine), 2.51 (s, 3H, Triazolopyrimidine-CH₃). ¹³C NMR (75 MHz, DMSO-*d*₆) δ 164.92, 164.64, 164.50, 164.45, 154.35, 150.03, 141.22, 137.70, 130.09, 129.51, 123.90, 121.83, 120.71, 119.44, 119.20, 118.57, 117.08, 116.80, 116.54, 100.15, 95.32, 47.71, 42.73, 25.00. Anal. Calcd. for C₂₆H₂₂ClF₄N₁₁: C, 52.05; H, 3.70; N, 25.68, Found: C, 52.43; H, 3.96; N, 25.31.

N2-(4-fluorophenyl)-6-(4-(5-methyl-[1,2,4]triazolo[1,5-a]pyrimidin-7-yl)piperazin-1-yl)-N4-(3-(trifluoromethyl)phenyl)-1,3,5-triazine-2,4diamine 10 (d).

White yellowish solid; yield: 68%; mp: 210-220 °C; ESI-MS: *m/z* = 566.2 [M+H]⁺; ¹H NMR (300 MHz, DMSO-*d*₆) δ 9.31 (s, 1H, -NH₁₀), 9.07 (s, 1H, -NH₉), 8.22 (s, 1H, Triazolopyrimidine-H_b), 7.97 (1H, Ar-H₇), 7.77 (d, *J* = 6.3 Hz, 1H, Ar-H₂), 7.51 (d, *J* = 6.6 Hz, 2H, Ar-H_{1,4}), 7.29 (1H, Ar-H₅), 7.06 (d, *J* = 7.5 Hz, 1H, Ar-H₃), 6.89 (2H, Ar-H_{6,8}), 6.39 (s, 1H, Triazolopyrimidine-H_a), 3.74 (8H, Piperazine), 2.28 (s, 3H, Triazolopyrimidine-CH₃). ¹³C NMR (75 MHz, DMSO-*d*₆) δ 172.43, 165.00, 164.70, 164.56, 157.16, 156.46, 154.39, 150.04, 141.39,

136.64, 130.00, 129.49, 126.57, 123.75, 122.96, 122.39, 118.30, 116.38, 115.51, 115.21, 95.28, 47.74, 42.71, 29.45. Anal. Calcd. for C₂₆H₂₃F₄N₁₁: C, 55.22; H, 4.10; N, 27.24; Found: C, 55.67; H, 4.19; N, 27.11.

N2-(3-chloro-4-fluorophenyl)-6-(4-(5-methyl-[1,2,4]triazolo[1,5-a]pyrimidin-7-yl)piperazin-1-yl)-N4-(p-tolyl)-1,3,5-triazine-2,4diamine 10 (e).

Off white solid; yield: 73%; mp: 270-280 °C; ESI-MS: m/z = 546.3 [M+H]⁺. ¹H NMR (300 MHz, DMSO-*d*₆) δ 9.37 (s, 1H, -NH₉), 9.20 (s, 1H, -NH₈), 8.45 (s, 1H, Triazolopyrimidine-H_b), 8.06 (d, *J* = 6.6 Hz, 2H, Ar-H_{5,6}), 7.58 (d, *J* = 7.8 Hz, 2H, Ar-H_{4,7}), 7.31 (s, 1H, Ar-H₃), 7.11 (d, *J* = 8.1 Hz, 2H, Ar-H_{1,2}), 6.62 (s, 1H, Triazolopyrimidine-H_a), 3.96 (8H, Piperazine), 3.31 (s, 3H, Toulidine-CH₃), 2.27 (s, 3H, Triazolopyrimidine-CH₃). ¹³C NMR (75 MHz, DMSO-*d*₆) δ 173.38, 164.98, 164.70, 164.42, 157.16, 154.38, 150.05, 137.96, 137.63, 135.65, 131.52, 129.35, 121.48, 120.95, 119.13, 117.04, 116.76, 108.53, 95.29, 47.78, 42.66, 25.06, 20.87. Anal. Calcd. for C₂₆H₂₅ClFN₁₁: C, 57.19; H, 4.62; N, 28.22, Found: C, 57.34; H, 4.55; N, 28.29.

4.1.8. Procedure for the synthesis of tri-substituted triazine piperazine compound 10 f

A mixture of piperazine (1.1 equiv), compound **3** (1.0 equiv) and K₂CO₃ (1.2 equiv) in 1,4-dioxane was reflux at 100 °C for 10-12 hrs. After the completion of reaction monitored by TLC, the reaction mixture was filtered and washed with 1,4-dioxane. The filtrate was vacuum dried and obtained the crude product. The obtained crude was further purified by column chromatography by 10% EtOAc/ Hexane to obtain the pure tri-substituted triazine piperazine **10 f** compound.

N2-cyclopropyl-6-(piperazin-1-yl)-N4-(3-(trifluoromethyl)phenyl)-1,3,5-triazine-2,4diamine 10 (f).

Milky white solid; yield: 81%; mp: 210-220 °C; Anal. Calcd. for C₁₇H₂₀F₃N₇: C, 53.82; H, 5.31; N, 25.84, Found: C, 52.98; H, 5.38; N, 25.87. ¹H NMR (400 MHz, DMSO-*d*₆) δ 9.50 (s, 1H, -NH₆), 8.69 (s, 1H, -NH₅), 7.78 (s, 1H, Cyclopropyl-H₇), 7.40 (2H, Ar-H_{2,4}), 7.18 (d, *J* = 7.2 Hz, 2H, Ar-H_{1,3}), 3.76 (s, 8H, Piperazine), 3.40 (s, 5H, Cyclopropyl-H_{8,9} & Piperazine-H₁₀). ¹³C NMR (100 MHz, DMSO-*d*₆) δ 167.49, 164.71, 142.02, 129.77, 126.29, 123.59, 123.12, 120.88, 117.75, 116.04, 43.03, 23.92, 14.49, 6.73.

4.2. Docking Protocol

The docking and scoring of ligands with AChE and BuChE proteins were accomplished using ParDOCK module of *Sanjeevini* drug design suite which is based on physico-chemical descriptors [20][21]. We used a rigid docking module for the preparation of reference protein complex and ligand in a force-field compatible manner as an input file. Docking of ligand molecule at the active site cavity of AChE and BuChE was done by using all atom energy based Monte Carlo algorithm which minimizes and scores the docked complex. The docked complexes were further minimized using the parallel version of sander module of AMBER [36], predicted binding free energy of docked poses are obtained using Bappl scoring function[37]. The docked structures were visualized using chimera [38].

4.3. Biological activity

4.3.1. In vitro inhibition studies on AChE and BuChE

The inhibitory activity of target compounds on AChE and BuChE was assessed using spectroscopic method of Ellman *et al.* [22]. Acetylcholinesterase (AChE, E.C. 3.1.1.7, from *electric eel*), butyrylcholinesterase (BuChE, E.C. 3.1.1.8, from *equine serum*), 5,5'- dithiobis-(2-

nitrobenzoic acid) (Ellman's reagent, DTNB), acetylthiocholine iodide (ATC), butyrylthiocholine iodide (BTC), donepezil and tacrine were purchased from Sigma Aldrich. The compounds were dissolved in DMSO and diluted using 0.1 M $\text{KH}_2\text{PO}_4/\text{K}_2\text{HPO}_4$ phosphate buffer (pH 8.0) to yield corresponding test concentrations (0.001-100) μM . Enzyme solutions were prepared by dissolving lyophilized powder in double-distilled water. The assay medium (1 ml) consisted of phosphate buffer (pH 8.0), 25 μl of AChE (0.22 U/ml) or 25 μl of BuChE (0.06 U/ml) and 100 μl of various concentrations of test compounds which was allowed to stand for 5 min before 100 μl of 0.01 M DTNB were added. A positive control of donepezil and tacrine were used in the same range of concentrations. The reaction was initiated by addition of 20 μl of the 0.075 M substrate solution (ATC/BTC) and exactly 2 min after substrate addition the absorption was measured at 25 °C at 412 nm. Assays were carried out with a blank containing all components except AChE or BuChE in order to account for non-enzymatic reaction. The concentration of compound producing 50% of enzyme activity inhibition (IC_{50}) was calculated by nonlinear regression analysis of the response-concentration (log) curve, using the Graph Pad Prism 5 program. All samples were assayed in triplicate.

4.3.2. Kinetic characterization of AChE inhibition

To obtain estimates of the mechanism of action of compounds **9a** and **9b**, reciprocal plots of $1/V$ vs $1/[S]$ were constructed at different concentrations of the substrate acetylthiocholine (0.05-0.50 mM) by using Ellman's method. Test compound was added into the assay solution and pre-incubated with the enzyme at 37 °C for 15 min, followed by the addition of substrate. Kinetic characterization of the hydrolysis of ATC catalyzed by AChE was carried out spectrometrically at 412 nm. V_{max} and K_m values of the Michaelis-Menten kinetics were calculated through nonlinear regression from substrate-velocity curves. Linear regression was

used for calculating the Lineweaver-Burk plots. Data analysis was performed with Graph Pad Prism 5 software (San Diego, CA, USA).

4.3.3. *Oxygen Radical Absorbance Capacity (ORAC-FL) Assay*

The antioxidant activity was determined by the oxygen radical absorbance capacity-fluorescein (ORAC-FL) assay. 2,2'-Azobis- (amidinopropane) dihydrochloride (AAPH), (±)-6-hydroxy-2,5,7,8- tetramethylchromane-2-carboxylic acid (trolox), and fluorescein (FL) were purchased from Sigma-Aldrich. All the assays were conducted with 75 mM phosphate buffer (pH 7.4), and the final reaction mixture was 200 µl. Antioxidant (20 µl) and FL (120 µl; 70 nM, final concentration) solutions were placed in a black 96-well microplate (96F untreated, Nunc). The mixture was incubated for 15 min at 37 °C, and then AAPH solution (60 µl, 12 mM, final concentration) was added rapidly using a multichannel pipette. The microplate was immediately placed in the TECAN multimode reader and the fluorescence was measured every 60 s for 120 min with excitation at 485 nm and emission at 520 nm. Trolox was used as a standard (1-10 µM, final concentration). A blank (FL + AAPH) using phosphate buffer instead of antioxidant and Trolox calibration were carried out in each assay. The samples were measured at different concentrations (0.5-10 µM). All reaction mixtures were prepared in triplicate, and at least three independent runs were performed for each sample. The antioxidant curves (fluorescence versus time) were normalized to the curve of the blank (without antioxidant). The net AUC corresponding to a sample was calculated by subtracting the AUC corresponding to the blank. Regression equations between net AUC and antioxidant concentration were calculated for all samples. ORAC-FL values were expressed as trolox equivalents by using the standard curve calculated for each assay, where the ORAC-FL value of trolox was taken as 1.

4.3.4. *Self-mediated A β ₁₋₄₂ aggregation assay*

The inhibition of self-induced A β ₁₋₄₂ aggregation was measured using a thioflavin T (ThT)-based fluorometric assay. Briefly, commercially available A β ₁₋₄₂ peptide was first treated with hexafluoroisopropanol (HFIP) at 5mg/ml to avoid self-aggregation. The peptide solution was then incubated for 24 h at room temperature and the solvent was evaporated under a stream of nitrogen until a clear film remained in the test tube. The HFIP pretreated A β ₁₋₄₂ sample was then resolubilized in DMSO to have a stable stock solution of 5 mM. Stock solutions of test compounds were prepared in DMSO and further diluted with 50 mM phosphate buffer phosphate buffer solution (pH 7.4) to achieve the desired concentrations. For the inhibition of self-mediated A β ₁₋₄₂ aggregation experiment, A β ₁₋₄₂ peptide (20 μ l, 25 μ M, final concentration) was incubated with 20 μ l of test compounds at different concentrations ranging from 5 to 50 μ M at 37°C for 24 h. Blanks containing 50 mM phosphate buffer (pH 7.4) instead of A β with or without inhibitors were also carried out. After incubation, samples were diluted to a final volume of 200 μ l with 50 mM glycine-NaOH buffer (pH 8.0) containing ThT (5 μ M). Fluorescence was measured on a TECAN infinite mutimode plate reader with excitation and emission wavelengths of 450 nm and 485 nm, respectively. The percent inhibition of aggregation was calculated by the following formula: $(1-IF_i/IF_c) \times 100\%$, where IF_i and IF_c are the fluorescence intensities obtained for A β in the presence and absence of inhibitors after subtracting the background fluorescence, respectively.

4.3.5. *CD spectroscopic analysis*

All CD measurements were performed by means of JASCO J-810 single beam spectropolarimeter, in the spectral range between 190 and 260 nm using a 0.5 mm path length cell at 25 °C. Spectra were recorded at 0.5 nm intervals with 1 nm bandwidth and 10 nm/min

scan speed. A β_{1-42} samples were prepared as described above. For CD measurements, the A β stock solution was diluted with 20 mM phosphate buffer (pH 7.4) to 20 μ M before use. A mixture of the peptide (10 μ l, 20 μ M, final concentration) with or without the tested compound (10 μ M) was incubated at 37°C for 24 hr. Background spectra were subtracted from scans of each A β sample spectrum.

4.3.6. Transmission electron microscopy (TEM) assay

For the metal-free experiment, the A β stock solution was diluted with 50 mM phosphate buffer (pH 7.4), which was incubated in the presence and absence of test compounds at 37 °C. The final concentrations of A β_{1-42} peptide and test inhibitors were 25 μ M, respectively. After 24 hours of incubation, aliquots (10 μ l) of the samples were placed on carbon-coated copper/rhodium grid. Each grid was negatively stained with 2% uranyl acetate solution for 1 min at room temperature. Excess staining solution was removed and the specimen was transferred for imaging with transmission electron microscopy (JEOL JEM-1400) [39].

4.3.7. Inhibition of AChE-induced A β_{1-42} peptide aggregation assay

The inhibitory potency of compounds on AChE-induced A β_{1-42} aggregation was determined by using thioflavin T (ThT) fluorescence method as described previously [40]. For co-incubation experiments, aliquots of AChE from *electric eel* (E.C. 3.1.1.7) and A β_{1-42} peptide in the presence or absence of test compounds were incubated for 6 h at 37°C. The final volume of each vial was 20 μ l, and the final concentrations of A β (dissolved in DMSO and diluted with 0.215 M sodium phosphate buffer, pH 8.0) and AChE (dissolved in 0.1 M sodium phosphate buffer, pH 8.0) were 25 μ M and 0.025 U, respectively. After the incubation period, 200 μ l of 5 μ M ThT in 50 mM glycine-NaOH buffer (pH 8.0) was added to each well. To quantify the amyloid fibril formation, ThT fluorescence was measured at excitation λ , 450 nm and

emission λ , 485 nm. The fluorescence intensities were compared, and the percent inhibition due to the presence of inhibitor was calculated by the following expression: $(1-IF_i/IF_c) \times 100\%$, where IF_i and IF_c are the fluorescence intensities obtained for $A\beta_{1-42}$ plus AChE in the presence and absence of inhibitor, respectively, minus the fluorescence intensities of respective blanks.

4.3.8. Metal binding studies

The study of metal chelation was performed using UV-vis spectrophotometer. To investigate the metal binding ability compound, the UV absorption spectra of tested compounds **9a** and **9b**, alone or in the presence of $CuSO_4$, $FeSO_4$, $FeCl_3$ or $ZnCl_2$ was recorded with wavelength ranging from 200 to 400 nm after incubating for 30 min in methanol at room temperature. The final volume of reaction mixture was 200 μ l, and the final concentrations of tested compound and metals were 50 μ M. The stoichiometry of the compound- Cu^{2+} complex was determined by employing Job's method. A fixed amount compound of **9a** and **9b** (50 μ M) was mixed with growing amounts of copper ion (5-100 μ M), and the difference UV-vis spectra were examined to investigate the ratio of ligand/metal in the complex.

4.3.9. Effects of 9a and 9b on metal-induced $A\beta_{1-42}$ aggregation and disaggregation experiments by ThT assay and TEM

The effects of compounds on metal-induced $A\beta_{1-42}$ aggregation were also determined by using ThT assay. The $A\beta_{1-42}$ stock solution was diluted with 25 μ M HEPES (pH 6.6) containing 150 μ M NaCl. 25 μ M $A\beta_{1-42}$ was incubated with 25 μ M Cu^{2+} in HEPES buffer at pH 6.6, without or with 50 μ M of tested compounds. The incubation was performed at 37 $^{\circ}$ C for 24 h. After incubation, the sample was diluted to a final volume of 200 μ l with 50 mM glycine-NaOH buffer (pH 8.0) containing ThT (5 μ M). The method for the detection of ThT fluorescence signal

was the same as that of self-mediated A β ₁₋₄₂ aggregation experiment. The TEM study was carried out as in the previous procedure [41].

4.3.10. ADME property prediction and TOPKAT analysis

ADME (Absorption, Distribution, Metabolism and excretion) properties were predicted using QikProp program, v. 3.5 (Schrödinger, LLC, New York). This gave an estimate of the physicochemical properties and the bioavailability of the compounds. Parameters such as polar surface area (PSA), solvent accessible surface area (SASA), CNS activity (Predicted central nervous system activity on a -2 (inactive) to +2 (active) scale), QPPCaco (Predicted apparent Caco-2 cell permeability in nm/s. Caco-2 cells is a model for the gut blood barrier), QPlogBB (Predicted brain/blood partition coefficient), QPPMDCK (Predicted apparent MDCK cell permeability in nm/s. MDCK cells are considered to be a good mimic for the blood-brain barrier), QPLogKhsa (Prediction of binding to human serum albumin), QPlogS (Predicted aqueous solubility) and percent human oral absorption (Predicted human oral absorption on 0-100% scale) were calculated. The acceptability of the compounds based on the Lipinski's rule of five were also estimated from the results. In addition, virtual toxicity risk assessment was performed using TOPKAT module of Accelrys Discovery studio 4.0. TOPKAT computes a probable value of toxicity for a submitted chemical structure from a quantitative structure-toxicity relationship (QSTR) equation. The triazine derivatives were monitored for dose dependent toxicity parameters including FDA and NTP rodent carcinogen models, skin irritancy, ocular irritancy, mutagenicity, aerobic biodegradability and developmental toxicity potential.

Acknowledgement

NH thanks UGC for Research Grant [File No. 37-591/2009(SR)]. EJ thanks Indian Council of Medical Research for the award of Research Associateship (Financial Assistance No.

BIC/II(39)/2015). MM thanks UGC for Central University Doctoral Fellowship and JK thanks to Council of Scientific and Industrial Research (CSIR), New Delhi (India), for the award of Senior Research Fellowship.

Appendix A. Supplementary data

Supplementary data associated with this article can be found in the online version, XXXXXXXX

References

- [1] A. Rauk, The chemistry of Alzheimer's disease, *Chemical Society Reviews*. 38 (2009) 2698.
- [2] M.L. Bolognesi, A. Gandini, F. Prati, E. Uliassi, From Companion Diagnostics to Theranostics: A New Avenue for Alzheimer's Disease?, *Journal of Medicinal Chemistry*. 59 (2016) 7759–70.
- [3] Z. Liang, B. Zhang, W.W. Su, P.G. Williams, Q.X. Li, C -Glycosylflavones Alleviate Tau Phosphorylation and Amyloid Neurotoxicity through GSK3 β Inhibition, *ACS Chemical Neuroscience*. 7 (2016) 912–923.
- [4] J. Nasica-Labouze, P.H. Nguyen, F. Sterpone, O. Berthoumieu, N.-V. Buchete, S. Coté, et al., Amyloid β Protein and Alzheimer's Disease: When Computer Simulations Complement Experimental Studies, *Chemical Reviews*. 115 (2015) 3518–3563.
- [5] M. Maqbool, M. Mobashir, N. Hoda, Pivotal role of glycogen synthase kinase-3: A therapeutic target for Alzheimer's disease, *European Journal of Medicinal Chemistry*. 107 (2016) 63–81.
- [6] D. dos Santos Pisoni, J. Sobieski da Costa, D. Gamba, C.L. Petzhold, A. César de Amorim Borges, M.A. Ceschi, et al., Synthesis and AChE inhibitory activity of new chiral tetrahydroacridine analogues from terpenic cyclanones, *European Journal of Medicinal Chemistry*. 45 (2010) 526–535.
- [7] V. Lozano, L. Aguado, B. Hoorelbeke, M. Renders, D. Schols, J. Balzarini, et al., Targeting HIV Entry through Interaction with Envelope Glycoprotein 120 (gp120): Synthesis and Antiviral Evaluation of 1,3,5-Triazines with Aromatic Amino Acids, 120 (2011) 5335–5348.

- [8] U.P. Singh, H.R. Bhat, P. Gahtori, Antifungal activity, SAR and physicochemical correlation of some thiazole-1,3,5-triazine derivatives, *Journal de Mycologie Médicale / Journal of Medical Mycology*. 22 (2012) 134–141.
- [9] P. Gahtori, S.K. Ghosh, P. Parida, A. Prakash, K. Gogoi, H.R. Bhat, et al., Antimalarial evaluation and docking studies of hybrid phenylthiazolyl-1,3,5-triazine derivatives: a novel and potential antifolate lead for Pf-DHFR-TS inhibition., *Experimental Parasitology*. 130 (2012) 292–9.
- [10] P. Gahtori, S.K. Ghosh, B. Singh, U.P. Singh, H.R. Bhat, A. Uppal, Synthesis, SAR and antibacterial activity of hybrid chloro, dichloro-phenylthiazolyl-s-triazines, *Saudi Pharmaceutical Journal*. 20 (2012) 35–45.
- [11] T.H. Corbett, W.R. Leopold, D.J. Dykes, B.J. Roberts, D.P. Griswold, F.M. Schabel, Toxicity and anticancer activity of a new triazine antifolate (NSC 127755)., *Cancer Research*. 42 (1982) 1707–15.
- [12] P. Singla, V. Luxami, K. Paul, Synthesis and in vitro evaluation of novel triazine analogues as anticancer agents and their interaction studies with bovine serum albumin., *European Journal of Medicinal Chemistry*. 117 (2016) 59–69.
- [13] E. Plebanek, F. Chevrier, V. Roy, T. Garenne, F. Lecaille, D. Warszycki, et al., Straightforward synthesis of 2,4,6-trisubstituted 1,3,5-triazine compounds targeting cysteine cathepsins K and S., *European Journal of Medicinal Chemistry*. 121 (2016) 12–20.
- [14] S. Federico, A. Ciancetta, N. Porta, S. Redenti, G. Pastorin, B. Cacciari, et al., 5,7-Disubstituted-[1,2,4]triazolo[1,5-a][1,3,5]triazines as pharmacological tools to explore the antagonist selectivity profiles toward adenosine receptors., *European Journal of Medicinal*

- Chemistry. 108 (2016) 529–41.
- [15] H. Bera, S. Chigurupati, Recent discovery of non-nucleobase thymidine phosphorylase inhibitors targeting cancer., *European Journal of Medicinal Chemistry*. 124 (2016) 992–1003.
- [16] W.G. Lewis, L.G. Green, F. Grynszpan, Z. Radić, P.R. Carlier, P. Taylor, et al., Click chemistry in situ: acetylcholinesterase as a reaction vessel for the selective assembly of a femtomolar inhibitor from an array of building blocks., *Angewandte Chemie (International Ed. in English)*. 41 (2002) 1053–7.
- [17] M. Maqbool, A. Manral, E. Jameel, J. Kumar, V. Saini, A. Shandilya, et al., Development of cyanopyridine–triazine hybrids as lead multitarget anti-Alzheimer agents, *Bioorganic & Medicinal Chemistry*. 24 (2016) 2777–2788.
- [18] J. Kumar, P. Meena, A. Singh, E. Jameel, M. Maqbool, M. Mobashir, et al., Synthesis and screening of triazolopyrimidine scaffold as multi-functional agents for Alzheimer's disease therapies, *European Journal of Medicinal Chemistry*. 119 (2016) 260–277.
- [19] K. Helmja, M. Vaher, T. Püssa, M. Kaljurand, Analysis of the stable free radical scavenging capability of artificial polyphenol mixtures and plant extracts by capillary electrophoresis and liquid chromatography–diode array detection–tandem mass spectrometry, *Journal of Chromatography A*. 1216 (2009) 2417–2423.
- [20] B. Jayaram, T. Singh, G. Mukherjee, A. Mathur, S. Shekhar, V. Shekhar, Sanjeevini: a freely accessible web-server for target directed lead molecule discovery, *BMC Bioinformatics*. 13 (2012) S7.
- [21] T. Singh, D. Biswas, B. Jayaram, AADS - An Automated Active Site Identification, Docking, and Scoring Protocol for Protein Targets Based on Physicochemical Descriptors,

- Journal of Chemical Information and Modeling. 51 (2011) 2515–2527.
- [22] G.L. Ellman, K.D. Courtney, V. Andres, R.M. Featherstone, A new and rapid colorimetric determination of acetylcholinesterase activity, *Biochemical Pharmacology*. 7 (1961) 88–95.
- [23] X. Huang, C.S. Atwood, M.A. Hartshorn, G. Multhaup, L.E. Goldstein, R.C. Scarpa, et al., The A β Peptide of Alzheimer's Disease Directly Produces Hydrogen Peroxide through Metal Ion Reduction, *Biochemistry*. 38 (1999) 7609–7616..
- [24] M. Rosini, E. Simoni, M. Bartolini, A. Tarozzi, R. Matera, A. Milelli, et al., Exploiting the lipoic acid structure in the search for novel multitarget ligands against Alzheimer's disease, *European Journal of Medicinal Chemistry*. 46 (2011) 5435–5442.
- [25] M.L. Bolognesi, A. Cavalli, C. Bergamini, R. Fato, G. Lenaz, M. Rosini, et al., Toward a rational design of multitarget-directed antioxidants: merging memquin and lipoic acid molecular frameworks., *Journal of Medicinal Chemistry*. 52 (2009) 7883–6.
- [26] A. Dávalos, C. Gómez-Cordovés, B. Bartolomé, Extending Applicability of the Oxygen Radical Absorbance Capacity (ORAC–Fluorescein) Assay, *Journal of Agricultural and Food Chemistry*. 52 (2004) 48–54.
- [27] F. Yang, G.P. Lim, A.N. Begum, O.J. Ubeda, M.R. Simmons, S.S. Ambegaokar, et al., Curcumin inhibits formation of amyloid beta oligomers and fibrils, binds plaques, and reduces amyloid in vivo., *The Journal of Biological Chemistry*. 280 (2005) 5892–901.
- [28] Lomakin, D.S. Chung, G.B. Benedek, D. Kirschner, D.B. Teplow, On the nucleation and growth of amyloid beta-protein fibrils: detection of nuclei and quantitation of rate constants., *Proceedings of the National Academy of Sciences of the United States of America*. 93 (1996) 1125–1129.

- [29] D.A. Kirschner, C. Abraham, D.J. Selkoe, X-ray diffraction from intraneuronal paired helical filaments and extraneuronal amyloid fibers in Alzheimer disease indicates cross-beta conformation., *Proceedings of the National Academy of Sciences of the United States of America*. 83 (1986) 503–7.
- [30] N.C. Inestrosa, A. Alvarez, C.A. Pérez, R.D. Moreno, M. Vicente, C. Linker, et al., Acetylcholinesterase accelerates assembly of amyloid-beta-peptides into Alzheimer's fibrils: possible role of the peripheral site of the enzyme., *Neuron*. 16 (1996) 881–91.
- [31] G. V De Ferrari, M.A. Canales, I. Shin, L.M. Weiner, I. Silman, N.C. Inestrosa, A structural motif of acetylcholinesterase that promotes amyloid beta-peptide fibril formation., *Biochemistry*. 40 (2001) 10447–57.
- [32] M. del Monte-Millán, E. García-Palomero, R. Valenzuela, P. Usán, C. de Austria, P. Muñoz-Ruiz, et al., Dual Binding Site Acetylcholinesterase Inhibitors: Potential New Disease-Modifying Agents for AD, *Journal of Molecular Neuroscience*. 30 (2006) 85–88.
- [33] L. Huang, C. Lu, Y. Sun, F. Mao, Z. Luo, T. Su, et al., Multitarget-Directed Benzylideneindanone Derivatives: Anti- β -Amyloid ($A\beta$) Aggregation, Antioxidant, Metal Chelation, and Monoamine Oxidase B (MAO-B) Inhibition Properties against Alzheimer's Disease, *Journal of Medicinal Chemistry*. 55 (2012) 8483–8492.
- [34] L. Schrödinger, QikProp, version 3.5, New York, (2012).
- [35] J. Kelder, P.D. Grootenhuys, D.M. Bayada, L.P. Delbressine, J.P. Ploemen, Polar molecular surface as a dominating determinant for oral absorption and brain penetration of drugs., *Pharmaceutical Research*. 16 (1999) 1514–9.
- [36] D.A. Pearlman, D.A. Case, J.W. Caldwell, W.S. Ross, T.E. Cheatham, S. DeBolt, et al., AMBER, a package of computer programs for applying molecular mechanics, normal

- mode analysis, molecular dynamics and free energy calculations to simulate the structural and energetic properties of molecules, *Computer Physics Communications*. 91 (1995) 1–41.
- [37] T. Jain, B. Jayaram, An all atom energy based computational protocol for predicting binding affinities of protein-ligand complexes, *FEBS Letters*. 579 (2005) 6659–6666.
- [38] E.F. Pettersen, T.D. Goddard, C.C. Huang, G.S. Couch, D.M. Greenblatt, E.C. Meng, et al., UCSF Chimera--a visualization system for exploratory research and analysis., *Journal of Computational Chemistry*. 25 (2004) 1605–12.
- [39] J.-S. Choi, J.J. Braymer, R.P.R. Nanga, A. Ramamoorthy, M.H. Lim, Design of small molecules that target metal-A β species and regulate metal-induced A β aggregation and neurotoxicity., *Proceedings of the National Academy of Sciences of the United States of America*. 107 (2010) 21990–5.
- [40] P. Meena, A. Manral, V. Nemaysh, V. Saini, F. Siraj, P.M. Luthra, et al., Novel insights into multitargeted potential of N'-(4-benzylpiperidin-1-yl)alkylamine derivatives in the management of Alzheimer's disease associated pathogenesis, *RSC Adv*. 6 (2016) 104847–104867.
- [41] A. Manral, V. Saini, P. Meena, M. Tiwari, Multifunctional novel Diallyl disulfide (DADS) derivatives with β -amyloid-reducing, cholinergic, antioxidant and metal chelating properties for the treatment of Alzheimer's disease., *Bioorganic & Medicinal Chemistry*. 23 (2015) 6389–403.

Abbreviations:

ACh	Acetylcholine
AChE	Acetylcholinesterase
BuChE	Butyrylcholinesterase
eqBuChE	Equine serum butyrylcholinesterase
AD	Alzheimer's disease
A β	Amyloid beta
AChEI	Acetylcholinesterase inhibitor
PAS	Peripheral anionic site
CAS	Catalytic active site
EeAChE	
SAR	Structure activity relationship
ORAC-FL	Oxygen radical absorbance capacity-fluorescein
ATC	Acetylthiocholine iodide
BTC	Butyrylthiocholine iodide
ThT Assay	Thioflavin T assay
QSTR	Quantitative structure-toxicity relationship